

1 **Measurement Report: Cloud condensation nuclei (CCN)**
2 **activity in the South China Sea from shipborne**
3 **observations during summer and winter of 2021: seasonal**
4 **variation and anthropogenic influence.**

5 Hengjia Ou¹, Mingfu Cai², Yongyun Zhang¹, Xue Ni¹, Baoling Liang³, Qibin Sun^{4,5},
6 Shixin Mai¹, Cuizhi Sun⁶, Shengzhen Zhou¹, Haichao Wang¹, Jiaren Sun², Jun Zhao¹

7 ¹School of Atmospheric Sciences, Guangdong Province Key Laboratory for Climate Change and Natural
8 Disaster Studies, Southern Marine Science and Engineering Guangdong Laboratory (Zhuhai), Sun Yat-
9 sen University, Zhuhai, Guangdong 519082, China

10 ²Guangdong Province Engineering Laboratory for Air Pollution Control, Guangdong Provincial Key
11 Laboratory of Water and Air Pollution Control, South China Institute of Environmental Sciences, MEE,
12 Guangzhou 510655, China

13 ³Guangzhou Sub-branch of Guangdong Ecological and Environmental Monitoring Center, Guangzhou
14 510006, China

15 ⁴Dongguan Meteorological Bureau, Dongguan, Guangdong, 523086, China

16 ⁵Dongguan Engineering Technology Research Center of Urban Eco-Environmental Meteorology,
17 Dongguan, Guangdong, 523086, China

18 ⁶Southern Marine Science and Engineering Guangdong Laboratory (Zhuhai), Zhuhai, Guangdong
19 519082, China

20
21 *Correspondence:* Mingfu Cai (caimingfu@scies.org) and Jun Zhao (zhaojun23@mail.sysu.edu.cn)

22

23 **Abstract**

24 Understanding seasonal variations in cloud condensation nuclei (CCN) activity and the impact of
25 anthropogenic emissions in marine environments is crucial for assessing climate change. This study
26 presents findings from two shipborne observations conducted in the South China Sea (SCS) during the
27 summer and winter of 2021. ~~In summer, higher particle number concentrations but lower mass~~
28 ~~concentrations of non-refractory submicron particles (NR-PM₁) were observed, driven by Aitken mode~~
29 ~~particle dominance. In contrast, winter showed a more balanced distribution between Aitken and~~
30 ~~Accumulation mode particles.~~ Summer particles were more hygroscopic, exhibiting higher activation
31 ratios (ARs) at ~~all~~ supersaturation (SS) levels. ~~Distinct air mass periods were identified: in summer,~~
32 ~~terrestrial air masses from Luzon ("Luzon" period), the Indochinese Peninsula ("Indochinese Peninsula"~~
33 ~~period), and marine air masses; in winter, periods were influenced by Mainland China ("Mainland China"~~
34 ~~period), a mix of Mainland China and marine air masses ("Mixed" period), and purely marine air masses.~~
35 The "Luzon" period in summer exhibited the highest particle number concentration, especially in the
36 Aitken mode, resulting in the highest CCN number concentration (N_{CCN}). Aerosol hygroscopicity was
37 higher during the "Indochinese Peninsula" period compared to the ~~"Luzon"~~ period, leading to a higher
38 ~~bulk~~ AR due to the combination of higher hygroscopicity and a greater fraction of accumulation mode
39 particles. The ~~"Mainland China"~~ period in winter showed a high nitrate fraction in the NR-PM₁, but the
40 inorganic fraction was similar to it in the ~~"Luzon"~~ period, resulting in comparable hygroscopicity at low
41 SS to the ~~"Luzon"~~ period. ~~However, smaller particle hygroscopicity was significantly lower in the~~
42 ~~"Mainland China" period compared to summer.~~ The ~~"Mixed"~~ period in winter exhibited a higher fraction
43 of accumulation mode particles, causing a higher ~~bulk~~ AR compared to the ~~"Mainland China"~~ period.
44 ~~Overall, summer terrestrial air masses increased Aitken particle and CCN concentrations, while winter~~
45 ~~terrestrial air masses led to a higher concentration of large particles and lower hygroscopicity of fine~~
46 ~~particles.~~ CCN closure analysis, considering aerosol composition and mixing state, revealed that summer
47 aerosol was primarily internally mixed, whereas smaller aerosol in winter was primarily externally mixed.
48 The potential effect of undetected sea salt may lead to an underestimation of aerosol hygroscopicity in
49 summer. This study highlights significant seasonal differences in aerosol properties and the impact of
50 different types of terrestrial air masses on CCN activity in the SCS, contributing to our understanding of
51 regional climate influences.

Formatted: Subscript

Deleted: In the summer, higher particle number concentrations but lower mass concentrations of non-refractory submicron particle matters (NR-PM₁) were observed. This was attributed to the dominance of particles in the Aitken mode during summer, whereas there was a more balanced distribution of Accumulation mode and Aitken mode particles in winter. ...

Deleted: high

Deleted: s, while hygroscopicity at low SS was similar in both seasons

Deleted: During the summer, three distinct periods were identified based on the air mass sources: terrestrial air masses from Luzon Island ("Luzon" period), and from the Indochinese Peninsula ("Indochinese Peninsula" period), and marine air masses. In winter, the periods were defined by terrestrial air masses from Mainland China ("Mainland China" period), a mix of Mainland China and marine air masses ("Mixed" period), and purely marine air masses.

Deleted: "

Deleted: "

Deleted: "Mainland China"

Deleted: "

Deleted: "

Deleted: However, hygroscopicity at small particle sizes was much lower in the "Mainland China" period than in the summer periods...

Deleted: "

Deleted: "

Deleted: "

Deleted: "

82 **1.Introduction**

83 Aerosols can act as cloud condensation nuclei (CCN), influencing cloud formation, lifespan, and
84 albedo, thus indirectly impacting global radiative balance (Fletcher et al., 2011; Albrecht, 1989). The
85 aerosol-cloud interaction currently represents the largest uncertainty in radiative forcing within climate
86 models, ranging from -1.7 to -0.3 W m⁻² (IPCC, 2021). This uncertainty can be attributed to the significant
87 spatiotemporal variability in the aerosol size distribution and the ability of atmospheric aerosol particles
88 acting as CCN (CCN activity) (Fitzgerald, 1973). Thus, field measurements of aerosol size distribution
89 and physicochemical properties are needed to better understand the radiative forcing exerted by
90 atmospheric aerosol particles.

91 Previous studies suggest that particle number size distribution (PNSD) is a primary factor
92 influencing CCN concentrations (Dusek et al., 2006; Rose et al., 2010; Pöhlker et al., 2016; Burkart et
93 al., 2011). The PNSD can account for 84–96% of the variability in the CCN concentrations (N_{CCN}) (Dusek
94 et al., 2006), while CCN activities may also play a significant role in the N_{CCN} (Quinn et al., 2008; Cai
95 et al., 2018; Ovadnevaite et al., 2017; Liu et al., 2018; Crosbie et al., 2015), which are primarily governed
96 by the particle size, chemical composition, mixing state, surface tension, and hygroscopicity (Köhler,
97 1936; Seinfeld and Pandis, 2016). Among these factors, the impact of hygroscopicity on CCN activities
98 has received great attention in recent years (Petters and Kreidenweis, 2007; Ajith et al., 2022; Rose et al.,
99 2010). Petters and Kreidenweis (2007) proposed the κ - Köhler theory based on the Köhler theory to
100 quantify the ability of aerosol particles to absorb moisture and become CCN based on the aerosol
101 hygroscopicity parameters (κ). Ajith et al. (2022) showed that 64% of particles can be activated as CCN
102 when κ is equal to 0.37, whereas when κ decreases to 0.23, only 48% of particles can be activated in the
103 tropical coastal area.

104 Significant seasonal variations in PNSD and hygroscopicity under both terrestrial and marine
105 environments were observed in previous field observations, leading to the seasonal variations in N_{CCN}
106 (Crosbie et al., 2015; Schmale et al., 2018; Burkart et al., 2011; Bougiatioti et al., 2009; Sihto et al., 2011;
107 Leena et al., 2016; Ross et al., 2003; Gras and Keywood, 2017; Quinn et al., 2019). Crosbie et al. (2015)
108 revealed that in the urban area of Arizona particles had larger sizes, higher hygroscopicity, and N_{CCN} was
109 also higher during winter, while a higher abundance of smaller particles was observed during summer
110 owing to stronger photochemical reactions. In pristine environments like mountain, coastal, and forested

Deleted:

Deleted: CCN concentrations

Formatted: Subscript

113 regions, seasonal variations in N_{CCN} and PNSD were more pronounced than urban and rural areas
114 (Schmale et al., 2018). Pöhlker et al. (2016) observed significant differences in N_{CCN} between the wet
115 and dry seasons in the Amazon rainforest, while the κ values remained relatively stable. They also noted
116 increased particle concentrations and aerosol hygroscopicity, both subject to the impact of long-range
117 transport originating from anthropogenic emissions. Observations in marine areas during different
118 seasons are relatively scarce compared with those in inland areas. Gras (1995) found that both particle
119 concentration and N_{CCN} in the Southern Ocean reached their peaks during summer and gradually decrease
120 to their valleys in winter. Quinn et al. (2019) showed that sea spray aerosols make a relatively significant
121 contribution to N_{CCN} only during winter in the Western North Atlantic, while in other seasons, the primary
122 contribution comes from biogenic aerosols oxidized from dimethyl sulfide (DMS). Zheng et al. (2020)
123 revealed that sulfate dominates the particle condensational growth to CCN sizes during summer in the
124 North Atlantic, while secondary organic aerosols played a significant role in particle growth throughout
125 all seasons. These results indicate that CCN activity and concentration could vary in a large range during
126 different seasons. Thus, further observations across different seasons in marine environments are needed
127 to enhance our understanding of marine CCN activities and their seasonal variations.

128 The South China Sea (SCS), located in Southeast Asia and bordered by China, the Indochinese
129 Peninsula, and Maritime Southeast Asia, is significantly influenced by air pollutants transported through
130 terrestrial air masses. Studies have shown that these pollutants play a crucial role in determining aerosol
131 concentration and properties in the region (Atwood et al., 2017; Xiao et al., 2017; Geng et al., 2019;
132 Liang et al., 2021; Sun et al., 2023; Qin et al., 2024). For instance, Xiao et al. (2017) reported that 69.7%
133 of nitrate and 57.5% of sulfate in the SCS originated from fossil fuel combustion, particularly coal
134 burning in Chinese coastal regions. Additionally, Liang et al. (2021) and Sun et al. (2023) observed an
135 increase in the organic fraction and concentration of submicron aerosols when the region was influenced
136 by terrestrial air masses from Mainland China and the Indochinese Peninsula in the northern SCS. Further
137 studies highlighted the variation in aerosol properties under different air mass influences. Atwood et al.
138 (2017) found a significant bimodal particle distribution with a κ value of 0.65 in the southern SCS under
139 marine air mass influence, whereas a unimodal distribution with a κ of 0.4 was observed under
140 continental air mass influence.

141 The SCS experiences a typical monsoon climate with distinct seasonal wind direction changes
142 (Wang et al., 2009). The northeast monsoon, occurring from November to March, is characterized by

143 stronger average wind speeds and longer period compared to the southwest monsoon, which dominates
144 from June to August. The transitional periods occur from April to May and September to October. During
145 the northeast monsoon, air pollutants are primarily transported to the SCS by terrestrial air masses from
146 China (Xiao et al., 2017; Liu et al., 2014; Geng et al., 2019). In contrast, during the summer, pollutants
147 mainly originate from terrestrial air masses from the Indochinese Peninsula and Maritime Southeast Asia
148 (Geng et al., 2019; Liang et al., 2021; Sun et al., 2023). These varying sources of anthropogenic emissions
149 exerts different impacts on CCN activity differently across seasons. Additionally, the fraction of high
150 cloud over the SCS varies from approximately 0.3 to 0.7 across different months, indicating that aerosol-
151 cloud interactions in the region may differ between seasons (Lu et al., 2022). However, due to limited
152 observational data, our understanding of seasonal variations in CCN activity in the SCS remains
153 incomplete. Conducting comprehensive observational studies on CCN activity across different seasons
154 is essential for improving our understanding of aerosol-cloud interactions on the SCS.

Deleted: high cloud

155 In this study, we conducted two shipborne observations in the SCS during summer (May 5–June 9,
156 2021) and winter (December 19–29, 2021). Our observations with online instruments focused on
157 measuring aerosol chemical composition, PNSD, and CCN activation in the region. Our results provide
158 valuable insights into the differences in CCN activity between winter and summer, as well as the
159 influence of different types of terrestrial air masses on CCN activity in the SCS across different seasons.

160 2. Methodology

161 2.1 Cruise information and onboard measurements

162 2.1.1 Cruise information

163 This study consists of two research cruises conducted during the summer and winter of 2021,
164 respectively. These two cruises were interdisciplinary scientific expeditions, integrating fields such as
165 marine geology, oceanography, and atmospheric environment. The primary objective in atmospheric
166 environment was to investigate the impact of summer and winter monsoons on the atmospheric
167 environment of the South China Sea (SCS). The summer and winter cruises were carried out respectively
168 by the vessels "Tan Kah Kee" and "Sun Yat-sen University". The "Tan Kah Kee" is an oceanographic
169 research vessel with a length of 77.7 meters, a beam of 16.24 meters, and a displacement of 3611 tons.
170 The "Sun Yat-sen University" is a comprehensive oceanographic training vessel with a total length of
171 114.3 meters, a beam of 19.4 meters, and a displacement of 6880 tons.

Deleted: different

174 The first cruise was from May 5th to June 9th, 2021. The cruise started from Xiamen Port and
175 traversed from the northern to the central-southern South China Sea, and then circled back near Hainan
176 Island, and finally returned to Xiamen Port. The second cruise was from December 19th to December
177 29th, 2021. It began from Gaolan Port in Zhuhai and reached the vicinity of Yongxing Island, and
178 ultimately returned to Gaolan Port (Fig. 1a). Unfortunately, due to adverse weather conditions, such as
179 strong winter monsoon winds causing poor sea conditions, and the fact that it was the first scientific
180 deployment of the research vessel Sun Yat-sen University, the winter cruise had a shorter duration and
181 covered a narrower spatial range, remaining only in the northern SCS (Fig. S1), compared to the summer
182 cruise. On both cruises, most of the instruments were housed in a single compartment and the sampling
183 lines were extended from the window of the compartment to the height of the ship's bridge (~17 m above
184 sea level) (Fig. 1a).

Deleted: Unfortunately, due to adverse weather conditions, such as strong winter monsoon winds causing poor sea conditions, and the fact that it was the first scientific deployment of the research vessel Sun Yat-sen University, the winter cruise had a shorter duration and covered a narrower spatial range compared to the summer cruise.

185 2.1.2 Size-resolved cloud condensation nuclei activity measurement

186 The size-resolved CCN activity was measured with a combination of a scanning mobility particle
187 sizer (SMPS) system and a cloud condensation nuclei counter (model CCNc-200, DMT Inc., USA), the
188 scanning mobility CCN analysis (SMCA) method initially proposed in Moore et al. (2010). The SMPS
189 system consisted of a differential mobility analyzer (DMA; model 3082, TSI, Inc.) and a condensation
190 particle counter (CPC; model 3756, TSI Inc.). The SMPS and the CCNc system were used to measure
191 PNSD and size-resolved CCN number concentration at a mobility size range of 10–500 nm and 10–593
192 nm in summer and winter campaign, respectively. Unfortunately, due to the malfunction of flow sensor
193 in the column B, only the data from column A is presented in this study. During the SMCA measurement,
194 the particles were first passed through a Nafion dryer to remove moisture, then neutralized using a
195 neutralizer. After that, they were subjected to size selection with a DMA. The particles were then split
196 between a CPC (1 L min⁻¹) for particle concentration measurement and a CCNc (0.5 L min⁻¹) for CCN
197 measurement at a specific supersaturation. To maintain sample flow through the DMA, dilution air (0.5
198 L min⁻¹) was added to the CPC inlet stream. The effect of the dilution air was accounted for in the PNSD
199 data processing (Fig. S2). The supersaturation (SS) of the CCNc was set at 0.2 %, 0.4 %, and 0.7 % in
200 summer campaign and 0.1%, 0.2 %, 0.4 %, and 0.7 % in winter campaign, respectively. Before the
201 measurements, the CCNc was calibrated with ammonium sulfate ((NH₄)₂SO₄) particles at each set SS.
202 Detailed description of the instrument configuration and calibration can be found in Cai et al. (2018).

Formatted: Indent: First line: 0 ch

Deleted: Although the CCNc-200 had two columns (column A and B), due to airflow issues in column B, only the data from column A is presented in this study.

Formatted: Font: Not Italic

Deleted:

Formatted: Font: Not Italic

213 **2.1.3 Aerosol chemical composition measurement**

214 The chemical composition of atmospheric non-refractory submicron particulate matter (NR-PM₁),
215 including sulfate, nitrate, organics, ammonium, and chloride, was measured using an online time-of-
216 flight ACSM (ToF-ACSM; Aerodyne Inc., USA). The sampling time of the ToF-ACSM was
217 approximately 10 min. The relative ionization efficiency (RIE) values of the instrument were calibrated
218 using ammonium nitrate (NH₄NO₃) and ammonium sulfate ((NH₄)₂SO₄) both before the start and after
219 the completion of the campaigns. The RIE values for ammonium were 3.31 and 3.33 during the summer
220 and winter, respectively, while the ones for sulfate were 1.02 and 0.81 during the summer and winter,
221 respectively. The collection efficiency (CE) was determined as shown in Sun et al. (2023) and time-
222 independent CE values were used in this study. Detailed CE calculation can be found in the
223 supplementary (Text S1, and Fig. S3). ~~The black carbon concentrations were measured with an~~
224 ~~aethalometer (AE33, Magee Scientific).~~

225 **2.1.4 Meteorological parameter measurements**

226 ~~The meteorological elements, including temperature, relative humidity, wind speed, and wind~~
227 ~~direction, were measured by the combined automatic weather station onboard the vessels. During the~~
228 ~~winter cruises, meteorology data before 12.22 was missed due to the calibration for the automatic weather~~
229 ~~station before 12.22. The timeseries of meteorological data were presented in Fig. S4.~~

230 **2.2 Data analysis**

231 **2.2.1 CCN activation**

232 The size-resolved number concentration of total ~~particle~~ and cloud condensation nuclei were
233 obtained from the SMPS and CCNc through the SMCA method. The activation diameter was determined
234 by fitting the activation ratio (AR, N_{CCN}/N_{CN}) and dry diameter at each supersaturation through the
235 following equation:

236
$$AR = \frac{B}{1 + \left(\frac{D_p}{D_{50}}\right)^C}, \quad (1)$$

237 where AR ~~indicates~~ the size-resolved AR, D_p represents dry particle diameter (nm); B, C, and D₅₀ are the
238 three fitting parameters, representing the asymptote, the slope, and the inflection point of the sigmoid,
239 respectively (Moore et al., 2010). The D₅₀ parameter, also known as the critical diameter, corresponds to

Deleted: S1

Deleted: The organic carbon (OC)/elemental carbon (EC) concentrations in PM_{2.5} were measured using a semi-continuous OC/EC analyzer (Model-4, Sunset Laboratory Inc., USA) based on the thermal optical transmittance technique and detailed measurement process can be found in Sun et al. (2023). The black carbon concentrations were measured with an aethalometer (AE33, Magee Scientific).

Deleted: Trace Gas and m

Deleted: The concentrations of trace gases (CO, O₃, SO₂, and NO_x) were measured using gas monitors (T400U, T100U, and T200U; Teledyne API Inc., USA).

Deleted: S2

Deleted: particle

Deleted:

Deleted: is

Formatted: Justified

256 the particle size at which 50% of the particles are activated at a specific SS. The fitting results from
257 SMCA method measured in this study are presented in Fig. S5.

258 The hygroscopicity parameter (κ) which represents CCN activity according to κ -Köhler equation is
259 calculated as follows (Petters and Kreidenweis, 2007):

$$260 \kappa = \frac{4A^3}{27D_{50}^3(\ln S_c)^2}, A = \frac{4\sigma_{s/a}M_w}{RT\rho_w} \quad (2)$$

261 where ρ_w is the density of pure water (about 997.04 kg m⁻³ at 298.15 K), M_w is the molecular weight of
262 water (0.018 kg mol⁻¹), $\sigma_{s/a}$ corresponds to the surface tension of the solution-air interface and is assumed
263 to be equal to the surface tension of pure water ($\sigma_{s/a}$ =0.0728 N m⁻¹ at 298.15 K), R is the universal gas
264 constant (8.314 J mol⁻¹ K⁻¹), T denotes thermodynamic temperature in kelvin (298.15 K), and D_{50} is the
265 critical diameter (in m). Additionally, it is noting that the estimated κ values refer to particles with the
266 D_{50} , which are the smallest particles that can be activated at a given SS.

267 During part of the summer measurement period, the D_{50} at 0.7% supersaturation ranged between 30
268 and 40. However, due to lower concentrations during these times, instrument noise introduced greater
269 measurement uncertainty, as demonstrated in Fig. S6. Consequently, the average D_{50} and κ at 0.7% SS
270 are not included in Table 1.

271 2.2.2 Closure Method

272 According to Petters and Kreidenweis. (2007), κ can be predicted by a simple mixing rule based
273 on chemical volume fractions:

$$274 \kappa_{sim} = \sum_i \varepsilon_i \kappa_i \quad (3)$$

275 where ε_i and κ_i are the volume fraction and hygroscopicity parameter for the specific dry
276 component in the mixture. We obtained ε from aerosol chemical composition measured by the ToF-
277 ACSM. In this study, κ for (NH₄)₂SO₄ (0.48), NH₄NO₃ (0.58), and NaCl (1.1) represent the κ of SO₄²⁻,
278 NO₃⁻, and Cl⁻ provided by the ToF-ACSM (Huang et al., 2022). Besides, the κ of organic was 0.1 at this
279 study according to Huang et al. (2022). The density of (NH₄)₂SO₄, NH₄NO₃, NaCl and organic are 1769
280 kg m⁻³, 1720 kg m⁻³, 2165 kg m⁻³, and 1400 kg m⁻³ (Huang et al., 2022; Gysel et al., 2007).

Deleted: S3

Formatted: Indent: First line: 0 ch

Formatted: Subscript

Formatted: Indent: First line: 2 ch

Formatted: Indent: First line: 2 ch

Deleted: from

Deleted: Nacl

Deleted: Nacl

Formatted: Underline, Font color: Dark Red

285 **2.2.3 CCN concentration and activation ratio calculation**

286 Due to the malfunction of the column B, the CCN concentration (N_{CCN}) was calculated based on the
 287 size-resolved AR at a specific SS from SMCA method and observed particle number concentration. It
 288 can be calculated by the following equation (Cai et al., 2018):

289
$$N_{CCN}(SS) = \int_0^{\infty} AR(SS, D_p) N_{CN}(D_p) dD_p \quad (4)$$

290 where $N_{CCN}(SS)$ is the CCN concentration at a specific SS, $AR(SS, D_p)$ is the ratio of N_{CCN} at a specific
 291 SS to N_{CN} on a specific diameter from the SMCA method and $N_{CN}(D_p)$ is the particle number
 292 concentration at a specific diameter (D_p). Due to the absence of direct measurements for total N_{CCN} , we
 293 refer to the N_{CCN} derived from Eq. (4) as observed values ($N_{CCN,obs}$) in this study. Previous research has
 294 shown that this method (size-resolved CCN from one column in CCNc-200) provides results closely
 295 matching those obtained from direct measurement (from another column in CCNc-200), supporting its
 296 reliability (Meng et al., 2014; Lathem and Nenes, 2011).

297 The N_{CCN} (referred as $N_{CCN,sim}(SS)$) can be predicted by D_{50} from closure method ($D_{50,sim}(SS)$)
 298 and N_{CN} according to following equation (Jurányi et al., 2011):

299
$$N_{CCN,sim}(SS) = \int_{D_{50,sim}(SS)}^{\infty} N_{CN}(D_p) dD_p \quad (5)$$

300 where the $D_{50,sim}(SS)$ is calculated based on the eq. (2) and (3).

301 The bulk AR at a specific SS can be calculated by:

302
$$AR(SS) = \frac{N_{CCN,obs}(SS)}{N_{CN,tot}} \quad (6)$$

303 where the $N_{CN,tot}$ represents the total particle number concentration.

304 To investigate the impact of the fraction and mixing state of aerosol on N_{CCN} , two CCN simulation
 305 scheme are applied in this study (Patel et al., 2021).

306 (1) Internal-mixed scheme: the aerosol composition from the ToF-ACSM was assumed to be size-
 307 independent and internally mixed. All aerosol has an identical chemical composition in the
 308 whole size range. N_{CCN} is calculated by N_{sim} and measured PNSD according to Eq. (2), Eq. (3),
 309 and Eq. (5) (Fig. S7a).

310 (2) External-mixed scheme: the aerosol composition from the ToF-ACSM was assumed to be size-
 311 independent and externally mixed. Four type of aerosol ((NH_4)₂SO₄, NH₄NO₃, NaCl and
 312 organic) are assumed to have a same proportion for all sizes. The D_{50} from each species was

Deleted: Since column B in the CCNc-200 cannot directly measure total CCN concentration

Deleted: T

Deleted: can be

Deleted: predicted

Deleted: particle number size distribution (PNSD) and D_{50}

Deleted:

Formatted: Justified, Tab stops: Not at 0 ch + 41.53 ch

Deleted: where $N_{CCN}(SS)$ is the CCN concentration at a specific SS, $AR(SS, D_p)$ is the ratio of N_{CCN} at a specific SS to N_{CN} on a specific diameter from the SMCA method and $N_{CN}(D_p)$ is the particle number concentration at a specific diameter (D_p).where $N_{CCN}(SS)$ is CCN concentration at a specific SS, $D_{50}(SS)$ is the activation diameter at a specific SS from the SMCA method or from closure method and $N_{CN}(D_p)$ is the particle number concentration under specific diameter from SMPS measurement.(Meng et al., 2014; Lathem and Nenes, 2011)...

Formatted: Font: Not Italic, Font color: Auto

Formatted: Subscript

Formatted: Subscript

Formatted: Subscript

Deleted: where $N_{CCN,sim}(SS)$ is simulated CCN concentration at a specific SS, $D_{50,sim}(SS)$ is the activation diameter at a specific SS from closure method and $N_{CN}(D_p)$ is the particle number density of specific diameter from SMPS measurement.

Deleted:

Deleted:
$$= \frac{\int_0^{\infty} AR(SS, D_p) N_{CN}(D_p) dD_p}{\int_0^{\infty} N_{CN}(D_p) dD_p} \int_{D_{50}(SS)}^{\infty} N_{CN}(D_p) dD_p$$

Deleted: (

Deleted: 5

Formatted: Normal

Deleted: It is noting that the AR here is bulk AR.

Deleted: ToF

Deleted: composition

Deleted: 4

343 calculated according to their κ values mentioned in 2.2.2. N_{CCN} is calculated according to the
344 Eq. (5) (Fig. S7b).

345 To access the simulation result from these two schemes, normalized mean bias (NMB) was used in
346 this study:

$$347 NMB = \frac{\sum(N_{CCN,sim} - N_{CCN,obs})}{\sum N_{CCN,obs}} \quad (6)$$

348 where $N_{CCN,sim}$ is the simulated N_{CCN} from two schemes, and $N_{CCN,obs}$ is the observed N_{CCN} .

349 2.2.4 Backward trajectory simulation and cluster analysis

350 Backward trajectory calculations were performed using the MeteInfo, an open-source software
351 (Wang, 2014) to determine potential source origins. Weekly GDAS1 (Global Data Assimilation System
352 at a resolution of 1°) files were downloaded from the NOAA Air Resource Laboratory (ARL) website
353 (<https://www.ready.noaa.gov/gdas1.php>). The calculation of backward trajectories is performed every
354 1 hour based on the location mentioned below, generating 72-hour backward trajectories at 500m.

355 To clarify the sources of air masses, the cluster analysis was applied in this study, which was
356 performed by TrajStat, a plug-in module of MeteInfo, based on k-means method
357 (http://meteothink.org/docs/trajstat/cluster_cal.html), According to the report by the China
358 Meteorological Administration (Chao et al., 2022), the summer monsoon in 2021 broke out during the
359 sixth pentad of May. Therefore, based on the timing of the monsoon onset and the actual trajectory of the
360 ship, we selected two representative midpoints of the ship track for backward trajectory calculations and
361 cluster analysis in summer; the midpoint of the ship's track before the onset of the summer monsoon
362 (May 5-23) and the midpoint of the track after the summer monsoon began (May 24-June 9). In the
363 winter cruise, backward trajectories calculation and cluster analysis was performed at two specific
364 locations: the ship's anchorage near Big Ten-thousand Mountain Island (December 19-22 and December
365 27-29) and the midpoint between Dawan Mountain Island and Yongxing Island (December 23-26). To
366 ensure the accuracy of the backward trajectory calculations and cluster analysis, we compared the
367 trajectories at the midpoints with those from the ship's actual locations to verify consistency in air mass
368 sources (Fig. S8). We further examined the trajectories for each cluster to verify their alignment with the
369 air mass origins they represent (Fig. S9). The results demonstrate that cluster analysis was well-
370 conducted. Additionally, figure S10 illustrates the average altitude variation as the age in hours increases
371 across different periods. During summer, the altitude of the clusters remained below 880 hPa, indicating

Deleted: <#>External-mixed scheme: the aerosol composition from the ToF-ACSM was assumed to be size-independent and externally mixed. Four type of aerosol ((NH₄)₂SO₄, NH₄NO₃, NaCl and organic) are assumed to have identical a proportion concentration at each size. N_{CCN} is calculated according to the Eq. (4)

Deleted: we applied

Deleted: in this study

Deleted: During the summer cruise, we conducted cluster analysis at two key locations

Deleted: outbreak

Deleted: 8

Deleted: 9

385 [that they resided within the boundary layer \(about 800 hPa\). While in winter, the altitude of the clusters](#)
386 [was higher than in summer, especially for the cluster during the mixed period \(peaked at about 755 hPa\).](#)
387 [However, these clusters were generally within or close to the boundary layer. These results suggest that](#)
388 [the back trajectories could represent the characteristics of the air masses originating from these specified](#)
389 [regions.](#)

Deleted: We further examined the trajectories for each cluster to confirm their alignment with the air mass origins they represent (Fig. S8). Additionally, Figure S9 illustrates the average pressure variation as the age in hours increases across different clusters.

390 2.2.5 Data quality control

391 To ensure reliable atmospheric samples in the SCS and mitigate the influence of research vessel
392 emissions, we applied the following data processing procedures (Huang et al., 2018; Cai et al., 2020;
393 Liang et al., 2021).

394 Firstly, we identified organic compounds, black carbon (BC), and small particulate matter (41.4 nm
395 particles) as indicators of ship emissions, recognizing their sudden peak values as indicative of the ship's
396 own emissions.

397 Secondly, we accounted for the relative positions of the ship's chimney and the sampling tube.
398 During the summer cruise, we excluded data corresponding to a relative wind direction (with respect to
399 the ship's bow) between 150° and 270° and a relative wind speed (with respect to the ship's speed) of less
400 than 2.5 m s⁻¹ (Fig. S11a, Fig. S12a1, and Fig. S13a-c). During the winter cruise, we excluded data for a
401 relative wind direction between 150° and 220° and a relative wind speed of less than 2.5 m s⁻¹ (Fig. S11b,
402 Fig. S12b1, and Figs. S13d-f).

Deleted: 4

Deleted: 5

Deleted: 6

Deleted: 4

Deleted: 5

Deleted: 6

403 Applying these criteria, 74.8% of the data in summer and 92.2% in winter (both at 10-minute
404 resolution) were classified as “clean” and retained for analysis. The timeseries of data before and after
405 quality control is shown in Fig. S14.

Deleted: 7

406 3. Results and discussion

407 3.1 CCN concentration and aerosol characteristics over SCS in summer and winter

408 Figure 2 presented the timeseries of PNSD (a1 and a2), NR-PM₁ mass concentrations and fractions
409 (b1 and b2, c1 and c2), number concentrations of CCN (d1 and d2), and hygroscopicity κ-values (e1 and
410 e2) during two campaigns in summer and winter. During the summer cruise, we observed two distinct
411 periods around the onset of the summer monsoon. The South China Sea (SCS) summer monsoon began
412 in the sixth pentad of May (Chao et al., 2022). In winter, the influence of the winter monsoon persisted

425 throughout the entire observation period (Fig. 1c). Despite our measurements being limited to the
426 northern SCS in winter, the impact of the Northeast Monsoon on the SCS was evident.

427 The average particle number concentration in summer (6966 cm^{-3}) was higher than in winter (4988
428 cm^{-3}), primarily due to the higher number concentration of Aitken-mode particles in summer (Fig. 3a-b).
429 In summer, particles were concentrated in smaller sizes, whereas in winter, particle size distribution was
430 relatively balanced between the Aitken mode (2185 cm^{-3}) and the accumulation mode (2176 cm^{-3}) (Fig.
431 3a-b).

432 The average mass concentration of NR-PM₁ was $3.76 \mu\text{g m}^{-3}$ in summer and increased to $9.39 \mu\text{g}$
433 m^{-3} in winter (Fig. 3c-d). In summer, the dominant aerosol component was sulfate (45.5%), followed by
434 organics (35.8%), ammonium (12.9%), nitrate (4.0%), and chloride (1.9%) (Fig. 3c), similar to the
435 pattern observed in the northern SCS during the summer of 2018 (Fig. 3e) (Liang et al., 2021). However,
436 in winter, organics became the predominant aerosol component (37%), with nitrate (22.2%) replacing
437 sulfate (18.9%) as the highest proportion of inorganic components (Fig. 3d). Although N_{CN} were higher
438 in summer than in winter, the particle volume size distribution indicates that a higher fraction of particles
439 was concentrated in larger size in winter, which significantly influenced mass concentration, resulting in
440 a higher NR-PM₁ concentration (Fig. S15).

441 The average number concentration of cloud condensation nuclei (N_{CCN}) in summer was higher than
442 in winter at all supersaturation (SS) levels (Table 1). The ratio of N_{CCN} between summer and winter was
443 smaller at high SS ($N_{\text{CCN,winter}}/N_{\text{CCN,summer}} = 0.51$ and 0.54 at 0.4% SS and 0.7% SS, respectively)
444 compared to low SS ($N_{\text{CCN,winter}}/N_{\text{CCN,summer}} = 0.62$ at 0.2% SS). Likely due to the significant difference in
445 number concentration of Aitken-mode particles between the two seasons (Fig. 3a-b). Compared to the
446 observation in the Yellow Sea, a region similarly influenced by terrestrial air masses from mainland
447 China, the N_{CCN} were lower in winter, while in summer, the N_{CCN} were more comparable to those
448 observed in the Yellow Sea (4821 cm^{-3} at 0.63% SS) (Park et al., 2018).

449 The aerosol hygroscopicity (κ) was higher in summer than that in winter (Table 1). Besides, the
450 hygroscopicity pattern varied between seasons: in summer, κ increased with SS (from 0.47 to 0.54
451 between 0.2% SS and 0.4% SS), while in winter, κ decreased with SS (from 0.50 to 0.15 between 0.1%
452 SS and 0.7% SS) (Fig. 3a-b). The winter κ pattern was similar to observations in the Western North
453 Pacific (Table 1) (Kawana et al., 2020). Additionally, the winter κ values were comparable to those in

Formatted: Subscript

Deleted:

Formatted: Subscript

Formatted: Subscript

Deleted: The absolute difference in the N_{CCN} between summer and winter was greater at high SS ($\Delta N_{\text{CCN}}=2099 \text{ cm}^{-3}$ and 1865 cm^{-3} at 0.4% SS and 0.7% SS, respectively) compared to low SS ($\Delta N_{\text{CCN}}=341 \text{ cm}^{-3}$ at 0.2% SS).

Formatted: Subscript

Formatted: Subscript

Formatted: Subscript

Deleted: the N_{CCN} in winterin ,the N_{CCN} more comparable

Formatted: Superscript

Deleted: it

Deleted: Aerosol hygroscopicity (κ) was similar at low SS but differed significantly at high SS between summer and winter (Table 1)

Deleted: .

Deleted: T

Deleted: 9

Deleted: 72

Formatted: Not Highlight

Formatted: Not Highlight

468 Guangzhou (Cai et al., 2020), adjacent to the SCS, indicating that the northern SCS is influenced by air
469 masses from Mainland China under the significant influence of the Northeast Monsoon during winter.

470 3.2 Anthropogenic influence on CCN concentration in different season

471 Cluster analysis revealed distinct periods influenced by various air masses. In summer, three
472 terrestrial air mass sources were identified: Luzon Island (referred to as “Luzon”), Palawan Island, and
473 the Indochinese Peninsula, along with a marine air mass source (Fig. 4a). Given the limited influence of
474 air masses from Palawan Island, this period was excluded from the study. Consequently, the study
475 focused on periods dominated by air masses from Luzon (“Luzon” period), the Indochinese Peninsula
476 (“Indochinese Peninsula” period), and marine sources (“Marine-s” period). In winter, the air mass
477 sources included Mainland China, a mixture of Mainland China and the South China Sea (referred to as
478 “Mixed”), and a marine source (Fig. 4b). These were classified as the “Mainland China” period, “Mixed”
479 period, and “Marine-w” period, respectively.

480 As shown in figure 5, terrestrial air masses could significantly affect the aerosol chemical
481 composition in the SCS, resulting in higher NR-PM₁ mass concentration and a higher fraction of organic
482 compounds compared to those influenced by marine air masses. Additionally, the particles number
483 concentration in the accumulation mode and the N_{CCN} at low supersaturation (SS) were higher during
484 periods influenced by terrestrial air masses (“Luzon” period) than those during marine air mass periods
485 (Table 2). Notably, we were able to obtain an accurate D₅₀ at 0.7% supersaturation only during the “Luzon”
486 period in summer. Due to the relatively lower hygroscopicity compared to other summer periods, the
487 corresponding D₅₀ at 0.7% SS ranged between 40 and 60 nm, with relatively high concentration of CN
488 and CCN (Fig. S6), allowing for a more precise measurement of D₅₀. As a result, the κ at 0.7% SS shown
489 in Fig. 7 was specific to the Luzon period in summer.

490 In summer, the “Luzon” period exhibited the highest N_{CN}, attributed to the elevated particle
491 concentration in the Aitken mode, compared to all other periods in both summer and winter (Fig. 6a and
492 Table 1). This high fraction of Aitken mode particles led to the lowest bulk AR among the summer
493 periods (Fig. 7a), as a larger fraction of particles centered on a size range lower than the D₅₀ (Fig. 7b).
494 Furthermore, the prevalence of a higher fraction of Aitken mode particles during terrestrial air mass
495 periods is commonly correlated with the influence of fresh anthropogenic emissions (Beddows et al.,
496 2015), which could lower the hygroscopicity and consequently suppress the bulk AR.

Deleted: Based on cluster analysis, we identified periods affected by different types of air masses. In summer, three terrestrial air mass sources were confirmed: from Luzon Island (referred to as “Luzon”), Palawan Island, and the Indochinese Peninsula, along with a marine air mass source (Fig. 4a). Due to the small fraction of air masses from Palawan Island, this period was excluded from the study. Consequently, the periods affected by air masses from Luzon, the Indochinese Peninsula, and marine sources were referred to as the “Luzon” period, “Indochinese Peninsula” period, and “Marine-s” period, respectively. In winter, the identified air mass sources included Mainland China, a Mainland China-SCS mixed source (referred to as “Mixed”), and a marine source (Fig. 4b). These were named as the “Mainland China” period, “Mixed” period, and “Marine-w” period, respectively.

Formatted: Font: Not Italic

Formatted: Font: Not Italic

Deleted: Notably, we were able to obtain an accurate D₅₀ at 0.7% supersaturation only during the “Luzon” period in summer, due to its relatively lower hygroscopicity compared to other summer periods. As a result, the κ at 0.7% SS shown in Fig. 7 was specific to the Luzon period in summer.

Deleted: Terrestrial air masses significantly affected the marine atmosphere in the SCS, resulting in higher NR-PM₁ mass concentration and a higher fraction of organic compounds compared to those influenced by marine air masses (Fig. 5). Additionally, the number concentration of particles (N_{CN}) in the accumulation mode and the number concentration of cloud condensation nuclei (N_{CCN}) at low supersaturation (SS) were higher during periods influenced by terrestrial air masses than those during marine air mass periods (Table 2).

Deleted: activation ratio (

Deleted:)

530 In the “Indochinese Peninsula” period, the N_{CN} was lower than it in the “Marine-s” period (Table
531 2). This difference was mainly due to the variation of Aitken mode particles, while accumulation mode
532 particles were higher during the “Indochinese Peninsula” period than in “Marine-s” period (Table 2). The
533 “Marine-s” period primarily occurred during the transition phase before the onset of summer monsoon,
534 when wind direction shifted from east (Luzon Island direction) to southwest (Indochinese Peninsula
535 direction). Anthropogenic emissions from Luzon Island still affected the marine atmosphere, leading to
536 higher concentrations of Aitken mode particles compared to the “Indochinese Peninsula” period (Table
537 2). The higher fraction of accumulation mode particles and higher hygroscopicity during the
538 “Indochinese Peninsula” period resulted in a higher bulk AR compared to the “Luzon” period. Despite a
539 higher organic fraction in NR-PM₁ during the “Indochinese Peninsula” period (Fig. 5), hygroscopicity
540 was still higher due to a higher oxidation degree of organics, indicated by a higher m/z 44 to 43 ratio
541 (5.87 compared to 5.60 in the “Luzon” period) (Lambe et al., 2011; Jimenez et al., 2009). Additionally,
542 higher wind speeds during this period (7.26 m s⁻¹ compared to 3.18 m s⁻¹ in the “Luzon” period) led to
543 a higher fraction of sea salt (Huang et al., 2022), resulting in a higher aerosol hygroscopicity. Unfortunately,
544 owing to instrument limit, sea salt cannot be detected by the ToF-ACSM.

545 In winter, nitrate accounted for the highest fraction of NR-PM₁ (25.4%) during the “Mainland
546 China” period compared to other periods (Fig. 5d). Due to similar hygroscopicity between nitrate and
547 sulfate, as well as comparable inorganic fractions between the “Mainland China” and “Luzon” periods,
548 κ at 0.2% SS was also similar between these two periods (0.30 and 0.33, respectively) (Fig. 7b). However,
549 aerosol hygroscopicity at small sizes was much lower in the “Mainland China” period than in the “Luzon”
550 period (Fig. 7b), contributing to the low bulk AR in the “Mainland China” period (Fig. 7a). The BC mass
551 concentration was higher during the “Mainland China” period (2.25 $\mu\text{g m}^{-3}$) compared to the “Luzon”
552 period (0.72 $\mu\text{g m}^{-3}$). This suggests that the lower hygroscopicity in smaller particles during the
553 “Mainland China” period may be attributed to a larger fraction of hydrophobic BC. Additionally,
554 hygroscopicity at smaller sizes was consistently lower across all winter periods, including the “Mainland
555 China” period, compared to summer. This phenomenon may be related to the reduced sulfate fraction in
556 smaller sizes during winter, as sulfate production via DMS oxidation is diminished due to lower sea
557 surface temperatures in winter (18.0°C) compared to summer (29.3°C), which in turn inhibits DMS
558 production by phytoplankton (Bates et al., 1987). The similar fractions of Aitken mode and accumulation

Deleted: In summer, the “Luzon” period had the highest N_{CN} , particularly in the Aitken mode, among all periods in both summer and winter (Fig. 6a and Table 1). The high fraction of Aitken mode particles contributed to the lowest activation ratio (AR) among the summer periods (Fig. 7a), further exacerbated by low hygroscopicity during this period (Fig. 7b). This high fraction of Aitken mode particles likely indicates a high fraction of primary organic aerosol, which lowers aerosol hygroscopicity.

Deleted: The N_{CN} during the “Indochinese Peninsula” period was lower than during the “Marine-s” period (Table 2).

Deleted: primarily

Deleted: onset

Deleted: In winter, nitrate had the highest fraction in NR-PM₁ (25.4%) during the “Mainland China” period among other periods. Due to similar hygroscopicity between nitrate and sulfate and similar inorganic fractions between the “Mainland China” and “Luzon” periods, κ at 0.2% SS was comparable (0.30 and 0.33, respectively) (Fig. 7b).

Deleted: This lower hygroscopicity could be due to lower sulfate concentration, oxidized by DMS, in winter than in summer, as higher sea surface temperatures in summer (29.3°C) compared to winter (18.0°C) promote DMS production by phytoplankton (Bates et al., 1987).

583 particles indicated that PNSD could not fully explain the low bulk AR in the “Mainland China” period.
584 Overall, lower N_{CN} and bulk AR in the “Mainland China” period compared to the “Luzon” period resulted
585 in a lower N_{CCN} .

586 During the “Mixed” period, N_{CCN} was lower than in the “Mainland China” period, which can be
587 attributed to the decreased N_{CN} (Table 2). However, accumulation mode particles dominated, unlike in
588 other terrestrial air mass periods (Fig. 6), resulting in a significantly higher bulk AR compared to the
589 “Mainland China” period. Organic aerosol hygroscopicity was also higher during the “Mixed” period,
590 supported by a higher m/z 44 to 43 ratio (3.88 vs. 3.10 in the “Mainland China” period), which explains
591 the greater hygroscopicity despite a higher organic fraction in NR-PM₁. Additionally, the lower BC
592 concentration in the “Mixed” period (1.20 $\mu\text{g m}^{-3}$ vs. 2.25 $\mu\text{g m}^{-3}$ in the “Mainland China” period)
593 suggests a smaller BC fraction. Moreover, the higher wind speeds during the “Mixed” period (10.77 m
594 s⁻¹ vs. 7.14 m s⁻¹ in the “Mainland China” period) could have increased the sea salt fraction, further
595 enhancing aerosol hygroscopicity.

596 3.3 CCN closure analysis

597 The CCN closure study is widely used to assess the impact of various factors on CCN activity (Patel
598 et al., 2021; Cai et al., 2018; Meng et al., 2014; Deng et al., 2013). In this study, we applied two schemes
599 based on the CCN closure method, as described in Section 2.2.3, which consider aerosol composition
600 and mixing state. The fitting parameters and coefficient of determination (R^2) are presented in Table 3,
601 while the fitting plots for both schemes are shown in Figures S16 and S17. Besides, the NMB from these
602 schemes was presented in Fig. 8.

603 In summer, the NMB was always lower than 0, which indicated that simulated aerosol
604 hygroscopicity was lower than observed value (Fig. 8). Sea salt which cannot be detected by the ToF-
605 ACSM may account for higher fraction in summer due to low aerosol concentration in summer (Fig. 3c),
606 resulting in the underestimation of aerosol hygroscopicity. The NMB exhibits similar trends with changes
607 in SS in all three periods in summer. Better fitting result appeared at high SS, which indicated a greater
608 underestimation of the hygroscopicity of larger particles. Besides, “Internal-mixed” scheme had more
609 precious result than it in “External-mixed” scheme in summer (Fig. 8), suggesting the aerosol was
610 primary internally mixed in summer.

Deleted: L

Formatted: Subscript

Formatted: Subscript

Formatted: Subscript

Deleted: During the “Mixed” period, the N_{CCN} was lower than in the “Mainland China” period, attributed to decreased N_{CN} (Table 2). However, particles were primarily concentrated in the accumulation mode, distinct from other terrestrial air mass periods (Fig. 6), leading to a significantly higher AR than the “Mainland China” period. Organic aerosol hygroscopicity was higher during the “Mixed” period than the “Mainland China” period, supported by a higher m/z 44 to 43 ratio (3.88 compared to 3.10 in the “Mainland China” period), explaining the higher hygroscopicity despite a higher organic fraction in NR-PM₁. Additionally, lower BC concentration in the “Mixed” period (1.20 $\mu\text{g m}^{-3}$ compared to 2.25 $\mu\text{g m}^{-3}$ in the “Mainland China” period) suggested a lower fraction of BC, which was hydrophobic. Higher wind speeds in the “Mixed” period (10.77 m s⁻¹ compared to 7.14 m s⁻¹ in the “Mainland China” period) could increase sea salt fraction, further enhancing aerosol hygroscopicity

Deleted: CCN closure study was widely applied to investigate the impacts of different factors on the CCN activity...

Deleted: In this study, two schemes considering aerosol composition and mixing state based on CCN closure method mentioned in 2.2.3 were applied. The fitting parameter and coefficient of determination (R^2) was shown in Table 3 and the fitting plots from two schemes were shown in Fig. S8 and Fig. S9.

Deleted: two

Deleted: different

Deleted: “Luzon” and “Indochinese Peninsula”

Deleted: in

Deleted: in “Indochinese Peninsula” period, while it appeared in low SS in “Luzon” period (Fig. 8)

Deleted: indicated that aerosol fraction had different trend as particle size increased in these two periods

646 In winter, the “External-mixed” scheme always showed a better result than “Internal-mixed” scheme
647 at high SS (0.4% SS and 0.7% SS), indicating that particles in small size were mainly externally mixed.
648 Considering the low hygroscopicity of small-sized particles in winter, it is likely that a significant fraction
649 of these particles consists of externally mixed BC, which probably originated from fresh anthropogenic
650 emissions and remains unmixed with other inorganic salts and organics. As BC ages, inorganic and
651 organic components adhere to it, which would lead to the increase of diameter and particles tended to be
652 internally mixed (Sarangi et al., 2019). This transition resulted in higher hygroscopicity in large-sized
653 particle compared to the smaller-sized particles. Besides, overestimation of aerosol hygroscopicity at
654 high SS could be owing to a higher fraction of non- or less- hygroscopic component (such as organic and
655 BC) at small particle sizes. The predicted N_{CCN} at 0.1% SS are 20%-40% lower than the observed
656 concentrations, whereas the predictions at 0.2% SS more closely match the observed values (Fig. 8). This
657 discrepancy may be due to the higher fraction of sea salt in larger particles. However, due to instrumental
658 limitations, the ToF-ACSM cannot detect BC and sea salt. Future observations including BC and sea salt
659 are needed to better assess their effects on aerosol hygroscopicity in the South China Sea (SCS). In
660 addition, further study of size-resolved aerosol composition can also enhance the understanding on CCN
661 activity in the SCS.

Formatted: Subscript

Deleted: The predicted N_{CCN} at 0.1% SS are 10%-20% lower than the observed concentrations, whereas the predicted value at 0.2% SS more closely aligns with the observed concentrations (Fig. 8). It could be owing to the higher fraction of sea salt at larger particle size. However, due to instrument limitations, black carbon and sea salt cannot be detected by the ToF-ACSM. More observations containing sea salt and black carbon are needed in the future to better assess their effects on aerosol hygroscopicity in SCS.

662 4. Conclusion

663 In this study, we investigated the seasonal variations of cloud condensation nuclei (CCN) activity
664 in the South China Sea (SCS) and explored the impact of anthropogenic emissions. Shipborne
665 observations were conducted during the summer (May 5–June 9) and winter (December 19–29) of 2021.
666 We measured CCN activity, chemical composition, and particle number size distribution (PNSD) using
667 several onboard instruments, including a ToF-ACSM, a CCNc, an SMPS, and an AE33. Observations
668 included periods before and after the summer monsoon onset and periods influenced by the winter
669 monsoon.

Deleted: outbreak

670 Our results show that particle number concentration (N_{CN}) and CCN number concentration (N_{CCN})
671 were higher in summer than in winter, while the mass concentration of non-refractory submicron
672 particulate matter (NR- PM_{10}) was lower in summer. This difference is primarily attributed to the
673 predominance of Aitken mode particles in summer, contrasted with a higher concentration of

684 ~~accumulation mode particles in winter.~~ Additionally, aerosol hygroscopicity and ~~bulk AR~~ were found to
685 be higher in summer than in winter.

686 ~~Backward trajectory and cluster analyses identified distinct influences from various air masses. In~~
687 ~~summer, we identified periods affected by terrestrial air masses from Luzon Island (the "Luzon" period)~~
688 ~~and the Indochinese Peninsula (the "Indochinese Peninsula" period), alongside a period influenced by~~
689 ~~marine air masses (the "Marine-s" period). In winter, the periods were influenced by terrestrial air masses~~
690 ~~from Mainland China (the "Mainland China" period), a mix of Mainland China and marine sources (the~~
691 ~~"Mixed" period), and marine air masses (the "Marine-w" period). Terrestrial air mass periods exhibited~~
692 ~~higher NR-PM₁ mass concentrations, organic fractions, and N_{CCN}, particularly at low supersaturation,~~
693 compared to those influenced by marine air masses.

694 During the ~~"Luzon"~~ period, high N_{CCN} was observed, attributed to high N_{CN}, especially in the Aitken
695 mode. This high concentration in the Aitken mode resulted in a low ~~bulk AR~~ at 0.2% SS, indicating a
696 higher fraction of primary organic aerosol with low hygroscopicity. This caused lower overall
697 hygroscopicity compared to other summer periods. The lower ratio of m/z 44 to 43 also suggested a
698 lower oxidation degree of organics in this period. In the "Indochinese Peninsula" period, ~~higher fraction~~
699 ~~of the accumulation mode particles compared to~~ the "Luzon" period led to a higher ~~bulk AR~~, combined
700 with increased hygroscopicity.

701 ~~In winter, the "Mainland China" period was characterized by a high nitrate fraction in the NR-PM₁.~~
702 ~~The similar inorganic fractions in the NR-PM₁ between the "Mainland China" and "Luzon" periods~~
703 ~~resulted in comparable aerosol hygroscopicity at low supersaturation (0.2% SS). However, at higher~~
704 ~~supersaturation levels (0.4% and 0.7% SS), the "Mainland China" period demonstrated significantly~~
705 ~~lower hygroscopicity, which led to a reduced bulk AR at elevated supersaturation.~~ During the "Mixed"
706 period, accumulation mode particles predominated, leading to a high ~~bulk AR~~. This indicated an aging
707 process during transport, with more oxidized organics and higher aerosol hygroscopicity. The lower black
708 carbon (BC) fraction and the higher sea salt fraction from high wind speed contributed to higher
709 hygroscopicity in the "Mixed" period compared to the "Mainland China" period, despite the high organic
710 fraction.

711 The CCN closure analysis, considering aerosol composition and mixing state, revealed that aerosols
712 in summer were primarily internally mixed, while in winter, small-sized aerosols were primarily
713 externally mixed. This distinction is crucial for climate models predicting N_{CCN} in the SCS. The

Deleted: This can be attributed to the predominance of Aitken mode particles in summer, compared to the higher concentration of accumulation mode particles in winter.

Deleted: activation ratio (

Deleted:)

Deleted: Backward trajectory and cluster analysis identified distinct air mass influences. In summer, we confirmed periods affected by terrestrial air masses from Luzon Island ("Luzon" period) and the Indochinese Peninsula ("Indochinese Peninsula" period), as well as a period influenced by marine air masses ("Marine-s" period). In winter, the periods were influenced by terrestrial air masses from Mainland China ("Mainland China" period), mixed air masses from Mainland China and marine sources ("Mixed" period), and marine air masses ("Marine-w" period). Periods influenced by terrestrial air masses showed higher NR-PM₁ mass concentration, organic fraction, and N_{CCN}, especially at low supersaturation (SS),...

Formatted: Subscript

Formatted: Subscript

Deleted: "

Deleted: "

Deleted: a higher particle fraction in the accumulation mode...compared to compared to

Deleted: compared to

Formatted: Subscript

Formatted: Subscript

Deleted: activation ratio (AR)

Deleted: In winter, the "Mainland China" period showed a high nitrate fraction in NR-PM₁. Similar inorganic fractions in NR-PM₁ between the "Mainland China" and "Luzon" periods resulted in similar aerosol hygroscopicity at low SS (0.2% SS). However, at higher SS (0.4% SS and 0.7% SS), the "Mainland China" period exhibited much lower hygroscopicity, causing a lower AR at high SS.

746 underestimation of aerosol hygroscopicity in summer suggests that the effect of sea salt should be
747 considered.

748 Our study highlights significant seasonal differences in CCN activity in the SCS and the influence of
749 different types of terrestrial air masses. Future measurements including size-resolved aerosol
750 composition and obtain more precise measurements of BC and sea salt are needed to better understanding
751 CCN activity in this region. Additionally, our observation in winter focused on the CCN activity over the
752 northern SCS, while the influence of air masses from Mainland China in remote SCS was still unclear.
753 Further observations in remote SCS areas could help clarify the anthropogenic influence during winter
754 under the effect of the winter monsoon.

Deleted:

755

756 *Data availability.* Data from the measurements are available at [https://doi.org/](https://doi.org/10.6084/m9.figshare.25472545)
757 [10.6084/m9.figshare.25472545](https://doi.org/10.6084/m9.figshare.25472545) (Ou et al., 2024).

Deleted: Additionally, our observation in winter focused on the CCN activity over the northern SCS, while the influence of air masses from Mainland China in remote SCS was still unclear. Further observations in remote SCS areas could help clarify the anthropogenic influence during winter under the effect of the winter monsoon.

758

759 *Supplement.* The supplement related to this article is available online at xxx.

760

761 *Author contributions.* **HO, MC, and JZ** designed the research. **YZ, XN, BL, and CS** performed the
762 measurements. **HO, MC, QS, and SM** analyzed the data. **SZ and HW** provided useful comment on the
763 paper. **HO, MC, and JZ** wrote the paper with contributions from all co-authors.

764

765 *Competing interests.* The authors declare that they have no conflict of interest.

766

767 *Financial support.* This work was supported by National Natural Science Foundation of China (NSFC)
768 (Grant No. 42305123 and 42175115) and Basic and Guangzhou Applied Basic Research Foundation
769 (Grant No. 2023A1515012240 and 2024A1515030221).

770

771 *Acknowledgements.* Additional support from the crew of the vessels "Tan Kah Kee" and "Sun Yat-sen
772 University" is greatly acknowledged.

773

774

782 **Reference**

783 Ajith T. C., Kompalli, S. K., and Babu, S. S.: Role of Aerosol Physicochemical Properties on Aerosol
784 Hygroscopicity and Cloud Condensation Nuclei Activity in a Tropical Coastal Atmosphere, *ACS Earth
785 Space Chem*, 6, 1527-1542, doi:<https://doi.org/10.1021/acsearthspacechem.2c00044>, 2022.

786 Albrecht, B. A.: Aerosols, cloud microphysics, and fractional cloudiness, *Science*, 245, 1227-1230,
787 doi:<https://doi.org/10.1126/science.245.4923.1227>, 1989.

788 Atwood, S. A., Reid, J. S., Kreidenweis, S. M., Blake, D. R., Jonsson, H. H., Lagrosas, N. D., Xian, P.,
789 Reid, E. A., Sessions, W. R., and Simpas, J. B.: Size-resolved aerosol and cloud condensation nuclei
790 (CCN) properties in the remote marine South China Sea - Part 1: Observations and source classification,
791 *Atmos. Chem. Phys.*, 17, 1105-1123, doi:<https://doi.org/10.5194/acp-17-1105-2017>, 2017.

792 Bates, T. S., Cline, J. D., Gammon, R. H., and Kelly-Hansen, S. R.: Regional and seasonal variations in
793 the flux of oceanic dimethylsulfide to the atmosphere, *J. Geophys. Res. Oceans*, 92, 2930-2938,
794 doi:<https://doi.org/10.1029/JC092iC03p02930>, 1987.

795 [Beddows, D. C. S., Harrison, R. M., Green, D. C., and Fuller, G. W.: Receptor modelling of both particle
796 composition and size distribution from a background site in London, UK, *Atmos. Chem. Phys.*, 15,
797 10107-10125, doi:<https://doi.org/10.5194/acp-15-10107-2015>, 2015.](#)

798 Bougiatioti, A., Fountoukis, C., Kalivitis, N., Pandis, S. N., Nenes, A., and Mihalopoulos, N.: Cloud
799 condensation nuclei measurements in the marine boundary layer of the eastern Mediterranean: CCN
800 closure and droplet growth kinetics, *Atmos. Chem. Phys.*, 9, 7053-7066, doi:<https://doi.org/10.5194/acp-9-7053-2009>, 2009.

802 Burkart, J., Steiner, G., Reischl, G., and Hitzenberger, R.: Long-term study of cloud condensation nuclei
803 (CCN) activation of the atmospheric aerosol in Vienna, *Atmos Environ*, 45, 5751-5759,
804 doi:<https://doi.org/10.1016/j.atmosenv.2011.07.022>, 2011.

805 [Cai, M. F., Liang, B. L., Sun, Q. B., Zhou, S. Z., Chen, X. Y., Yuan, B., Shao, M., Tan, H. B., and Zhao,
806 J.: Effects of continental emissions on cloud condensation nuclei \(CCN\) activity in the northern South
807 China Sea during summertime 2018, *Atmos. Chem. Phys.*, 20, 9153-9167,
808 doi:<https://doi.org/10.5194/acp-20-9153-2020>, 2020.](#)

809 Cai, M. F., Tan, H. B., Chan, C. K., Qin, Y. M., Xu, H. B., Li, F., Schurman, M. I., Liu, L., and Zhao, J.:
810 The size-resolved cloud condensation nuclei (CCN) activity and its prediction based on aerosol

Moved (insertion) [1]

Formatted: Font: (Asian) +Body Asian (等线)

Deleted: Cai, M., Tan, H., Chan, C. K., Mochida, M., Hatakeyama, S., Kondo, Y., Schurman, M. I., Xu, H., Li, F., Shimada, K., Li, L., Deng, Y., Yai, H., Matsuki, A., Qin, Y., and Zhao, J.: Comparison of Aerosol Hygroscopicity, Volatility, and Chemical Composition between a Suburban Site in the Pearl River Delta Region and a Marine Site in Okinawa, *Aerosol Air Qual Res*, 17, 3194-3208, doi:<https://doi.org/10.4209/aaqr.2017.01.0020>, 2017.

819 hygroscopicity and composition in the Pearl Delta River (PRD) region during wintertime 2014, *Atmos.*
820 *Chem. Phys.*, 18, 16419-16437, doi:<https://doi.org/10.5194/acp-18-16419-2018>, 2018.

821 Chao, Q., Xiao, C., Li, W., Wang, L., Sun, L., Chen, X., Chen, Y., Li, Y., Gao, G., Liu, Y., Zhang, D., Ai,
822 W., Chen, Y., Cui, T., Dai, T., Feng, A., Guo, Y., Huang, D., Jiang, Y., Li, D., Li, M., Liu, B., Liu, Y., Lv,
823 Z., Mei, M., Wang, Q., Wang, Y., Yin, Y., Zeng, H., Zhang, Y., Zhai, J., Zhao, L., Zhi, R., Zhong, H.,
824 Zhou, X., Zhou, X., Zhu, X., and Wu, H.: *China Climate Bulletin* (2022), China Meteorological
825 Administration, https://www.cma.gov.cn/zfxgk/gknr/qxbg/202303/t20230324_5396394.html, 2022.

826 Choi, Y., Rhee, T. S., Collett, J. L., Park, T., Park, S.-M., Seo, B.-K., Park, G., Park, K., and Lee, T.:
827 Aerosol concentrations and composition in the North Pacific marine boundary layer, *Atmos Environ.*,
828 171, 165-172, doi:<https://doi.org/10.1016/j.atmosenv.2017.09.047>, 2017.

829 Crosbie, E., Youn, J. S., Balch, B., Wonaschutz, A., Shingler, T., Wang, Z., Conant, W. C., Betterton, E.
830 A., and Sorooshian, A.: On the competition among aerosol number, size and composition in predicting
831 CCN variability: a multi-annual field study in an urbanized desert, *Atmos Chem Phys*, 15, 6943-6958,
832 doi:<https://doi.org/10.5194/acp-15-6943-2015>, 2015.

833 Deng, Z. Z., Zhao, C. S., Ma, N., Ran, L., Zhou, G. Q., Lu, D. R., and Zhou, X. J.: An examination of
834 parameterizations for the CCN number concentration based on in situ measurements of aerosol activation
835 properties in the North China Plain, *Atmos. Chem. Phys.*, 13, 6227-6237,
836 doi:<https://doi.org/10.5194/acp-13-6227-2013>, 2013.

837 Dusek, U., Frank, G. P., Hildebrandt, L., Curtius, J., Schneider, J., Walter, S., Chand, D., Drewnick, F.,
838 Hings, S., Jung, D., Borrmann, S., and Andreae, M. O.: Size matters more than chemistry for cloud-
839 nucleating ability of aerosol particles, *Science*, 312, 1375-1378,
840 doi:<https://doi.org/10.1126/science.1125261>, 2006.

841 Fitzgerald, J. W.: Dependence of the Supersaturation Spectrum of CCN on Aerosol Size Distribution and
842 Composition, *J Atmos Sci*, 30, 628-634, doi:[https://doi.org/10.1175/1520-0469\(1973\)030](https://doi.org/10.1175/1520-0469(1973)030), 1973.

843 Fletcher, Squires, I. b. P., and Bowen, F. b. E. G.: *The Physics of Rainclouds*, 2011.

844 Geng, X. F., Zhong, G. C., Li, J., Cheng, Z. B., Mo, Y. Z., Mao, S. D., Su, T., Jiang, H. Y., Ni, K. W., and
845 Zhang, G.: Molecular marker study of aerosols in the northern South China Sea: Impact of atmospheric
846 outflow from the Indo-China Peninsula and South China, *Atmos Environ*, 206, 225-236,
847 doi:<https://doi.org/10.1016/j.atmosenv.2019.02.033>, 2019.

848 Gras, J. L.: CN, CCN and particle size in Southern Ocean air at Cape Grim, *Atmos Res*, 35, 233-251,
849 doi:[https://doi.org/10.1016/0169-8095\(94\)00021-5](https://doi.org/10.1016/0169-8095(94)00021-5), 1995.

850 Gras, J. L. and Keywood, M.: Cloud condensation nuclei over the Southern Ocean: wind dependence
851 and seasonal cycles, *Atmos. Chem. Phys.*, 17, 4419-4432, doi:<https://doi.org/10.5194/acp-17-4419-2017>,
852 2017.

853 Gysel, M., Crosier, J., Topping, D. O., Whitehead, J. D., Bower, K. N., Cubison, M. J., Williams, P. I.,
854 Flynn, M. J., McFiggans, G. B., and Coe, H.: Closure study between chemical composition and
855 hygroscopic growth of aerosol particles during TORCH2, *Atmos. Chem. Phys.*, 7, 6131-6144,
856 doi:<https://doi.org/10.5194/acp-7-6131-2007>, 2007.

857 Huang, S., Wu, Z. J., Poulain, L., van Pinxteren, M., Merkel, M., Assmann, D., Herrmann, H., and
858 Wiedensohler, A.: Source apportionment of the organic aerosol over the Atlantic Ocean from 53 degrees
859 N to 53 degrees S: significant contributions from marine emissions and long-range transport, *Atmos.*
860 *Chem. Phys.*, 18, 18043-18062, doi: 10.5194/acp-18-18043-2018, 2018

861 Huang, S., Wu, Z., Wang, Y., Poulain, L., Höpner, F., Merkel, M., Herrmann, H., and Wiedensohler, A.:
862 Aerosol Hygroscopicity and its Link to Chemical Composition in a Remote Marine Environment Based
863 on Three Transatlantic Measurements, *Environ. Sci. Technol.*, 56, 9613-9622,
864 doi:<https://doi.org/10.1021/acs.est.2c00785>, 2022.

865 *Ipcc: Annex I: Observational Products* [Trewin, B. (ed.)], in: *Climate Change 2021: The Physical Science*
866 *Basis. Contribution of Working Group I to the Sixth Assessment Report of the Intergovernmental Panel*
867 *on Climate Change*, edited by: Masson-Delmotte, V., Zhai, P., Pirani, A., Connors, S. L., Péan, C., Berger,
868 S., Caud, N., Chen, Y., Goldfarb, L., Gomis, M. I., Huang, M., Leitzell, K., Lonnoy, E., Matthews, J. B.
869 R., Maycock, T. K., Waterfield, T., Yelekçi, O., Yu, R., and Zhou, B., Cambridge University Press,
870 Cambridge, United Kingdom and New York, NY, USA, 2061–2086,
871 <https://doi.org/10.1017/9781009157896.015>, 2021.

872 Jimenez, J. L., Canagaratna, M. R., Donahue, N. M., Prevot, A. S., Zhang, Q., Kroll, J. H., DeCarlo, P.
873 F., Allan, J. D., Coe, H., Ng, N. L., Aiken, A. C., Docherty, K. S., Ulbrich, I. M., Grieshop, A. P., Robinson,
874 A. L., Duplissy, J., Smith, J. D., Wilson, K. R., Lanz, V. A., Hueglin, C., Sun, Y. L., Tian, J., Laaksonen,
875 A., Raatikainen, T., Rautiainen, J., Vaattovaara, P., Ehn, M., Kulmala, M., Tomlinson, J. M., Collins, D.
876 R., Cubison, M. J., Dunlea, E. J., Huffman, J. A., Onasch, T. B., Alfarra, M. R., Williams, P. I., Bower,
877 K., Kondo, Y., Schneider, J., Drewnick, F., Borrmann, S., Weimer, S., Demerjian, K., Salcedo, D., Cottrell,

878 L., Griffin, R., Takami, A., Miyoshi, T., Hatakeyama, S., Shimono, A., Sun, J. Y., Zhang, Y. M., Dzepina,
879 K., Kimmel, J. R., Sueper, D., Jayne, J. T., Herndon, S. C., Trimborn, A. M., Williams, L. R., Wood, E.
880 C., Middlebrook, A. M., Kolb, C. E., Baltensperger, U., and Worsnop, D. R.: Evolution of organic
881 aerosols in the atmosphere, *Science*, 326, 1525-1529, doi:<https://doi.org/10.1126/science.1180353>, 2009.
882 Kawana, K., Miyazaki, Y., Omori, Y., Tanimoto, H., Kagami, S., Suzuki, K., Yamashita, Y., Nishioka, J.,
883 Deng, Y. G., Yai, H., and Mochida, M.: Number-Size Distribution and CCN Activity of Atmospheric
884 Aerosols in the Western North Pacific During Spring Pre-Bloom Period: Influences of Terrestrial and
885 Marine Sources, *J Geophys Res-Atmos*, 127, e2022JD036690,
886 doi:<https://doi.org/10.1029/2022JD036690>, 2022.
887 Köhler, H.: The nucleus in and the growth of hygroscopic droplets, *Trans. Faraday Soc.*, 32, 1152-1161,
888 doi:<https://doi.org/10.1039/TF9363201152>, 1936.
889 Lambe, A. T., Onasch, T. B., Massoli, P., Croasdale, D. R., Wright, J. P., Ahern, A. T., Williams, L. R.,
890 Worsnop, D. R., Brune, W. H., and Davidovits, P.: Laboratory studies of the chemical composition and
891 cloud condensation nuclei (CCN) activity of secondary organic aerosol (SOA) and oxidized primary
892 organic aerosol (OPOA), *Atmos. Chem. Phys.*, 11, 8913-8928, doi:[https://doi.org/10.5194/acp-11-8913-](https://doi.org/10.5194/acp-11-8913-2011)
893 2011, 2011.
894 Lathem, T. L. and Nenes, A.: Water Vapor Depletion in the DMT Continuous-Flow CCN Chamber:
895 Effects on Supersaturation and Droplet Growth, *Aerosol Sci Tech*, 45, 604-615,
896 doi:<https://doi.org/10.1080/02786826.2010.551146>, 2011.
897 Leena, P. P., Pandithurai, G., Anilkumar, V., Murugavel, P., Sonbawne, S. M., and Dani, K. K.: Seasonal
898 variability in aerosol, CCN and their relationship observed at a high altitude site in Western Ghats,
899 *Meteorol Atmos Phys*, 128, 143-153, doi:<https://doi.org/10.1007/s00703-015-0406-0>, 2016.
900 Liang, B., Cai, M., Sun, Q., Zhou, S., and Zhao, J.: Source apportionment of marine atmospheric aerosols
901 in northern South China Sea during summertime 2018, *Environ. Pollut*, 289, 117948,
902 doi:<https://doi.org/10.1016/j.envpol.2021.117948>, 2021.
903 Liu, P., Song, M., Zhao, T., Gunthe, S. S., Ham, S., He, Y., Qin, Y. M., Gong, Z., Amorim, J. C., Bertram,
904 A. K., and Martin, S. T.: Resolving the mechanisms of hygroscopic growth and cloud condensation nuclei
905 activity for organic particulate matter, *Nat. Commun*, 9, 4076, doi:[Formatted: Font: \(Asian\) +Body Asian \(等线\)](https://doi.org/10.1038/s41467-018-
906 06622-2, 2018.</p></div><div data-bbox=)

907 [Liu, Y., Sun, L., Zhou, X., Luo, Y., Huang, W., Yang, C., Wang, Y., and Huang, T.:](#) A 1400-year
908 terrigenous dust record on a coral island in South China Sea, *Sci Rep*, 4, 4994,
909 doi:<https://doi.org/10.1038/srep04994>, 2014.

910 Lu, W., Yang, S., Zhu, W., Li, X., Cui, S., Luo, T., Han, L., and Shi, J.: Evaluation of High Cloud Product
911 of ECMWF Over South China Sea Using CALIOP, *Earth Space Sci*, 9, e2021EA002113,
912 doi:<https://doi.org/10.1029/2021ea002113>, 2022.

913 Meng, J. W., Yeung, M. C., Li, Y. J., Lee, B. Y. L., and Chan, C. K.: Size-resolved cloud condensation
914 nuclei (CCN) activity and closure analysis at the HKUST Supersite in Hong Kong, *Atmos. Chem. Phys.*,
915 14, 10267-10282, doi:<https://doi.org/10.5194/acp-14-10267-2014>, 2014.

916 Moore, R. H., Nenes, A., and Medina, J.: Scanning Mobility CCN Analysis-A Method for Fast
917 Measurements of Size-Resolved CCN Distributions and Activation Kinetics, *Aerosol Sci Tech*, 44, 861-
918 871, doi:<https://doi.org/10.1080/02786826.2010.498715>, 2010.

919 Ou, H., Cai, M., Zhang, Y., Ni, X., Liang, B., Sun, Q., Mai, S., Sun, C., Zhou, S., Wang, H., Sun, j., and
920 Zhao, J.: Measurement Report: Seasonal variation and anthropogenic influence on cloud condensation
921 nuclei (CCN) activity in the South China Sea: Insights from shipborne observations during summer and
922 winter of 2021 [dataset], doi:<https://doi.org/10.6084/m9.figshare.25472545>, 2024.

923 Ovadnevaite, J., Zuend, A., Laaksonen, A., Sanchez, K. J., Roberts, G., Ceburnis, D., Decesari, S.,
924 Rinaldi, M., Hodas, N., Facchini, M. C., Seinfeld, J. H., and O'Dowd, C.: Surface tension prevails over
925 solute effect in organic-influenced cloud droplet activation, *Nature*, 546, 637-641,
926 doi:<https://doi.org/10.1038/nature22806>, 2017.

927 [Park, M., Yum, S. S., Kim, N., Cha, J. W., Shin, B., and Ryoo, S.-B.:](#) Characterization of submicron
928 aerosols and CCN over the Yellow Sea measured onboard the Gisang 1 research vessel using the positive
929 matrix factorization analysis method, *Atmos Res*, 214, 430-441,
930 doi:<https://doi.org/10.1016/j.atmosres.2018.08.015>, 2018.

931 Patel, P. N. and Jiang, J. H.: Cloud condensation nuclei characteristics at the Southern Great Plains site:
932 role of particle size distribution and aerosol hygroscopicity, *Environ Res Commun*, 3,
933 doi:<https://doi.org/10.1088/2515-7620/ac0e0b>, 2021

934 Petters, M. D. and Kreidenweis, S. M.: A single parameter representation of hygroscopic growth and
935 cloud condensation nucleus activity, *Atmos. Chem. Phys.*, 7, 1961-1971, doi:[https://doi.org/10.5194/acp-](https://doi.org/10.5194/acp-7-1961-2007)
936 [7-1961-2007](https://doi.org/10.5194/acp-7-1961-2007), 2007.

Deleted: Liu, X. and Wang, J.: How important is organic aerosol hygroscopicity to aerosol indirect forcing?, *Environ. Res. Lett*, 5, 044010, doi:<https://doi.org/10.1088/1748-9326/5/4/044010>, 2010.

Formatted: Normal

941 Pöhlker, M. L., Pöhlker, C., Ditas, F., Klimach, T., Hrabec de Angelis, I., Araújo, A., Brito, J., Carbone,
942 S., Cheng, Y., Chi, X., Ditz, R., Gunthe, S. S., Kesselmeier, J., Könemann, T., Lavrič, J. V., Martin, S. T.,
943 Mikhailov, E., Moran-Zuloaga, D., Rose, D., Saturno, J., Su, H., Thalman, R., Walter, D., Wang, J., Wolff,
944 S., Barbosa, H. M. J., Artaxo, P., Andreae, M. O., and Pöschl, U.: Long-term observations of cloud
945 condensation nuclei in the Amazon rain forest – Part 1: Aerosol size distribution, hygroscopicity, and
946 new model parametrizations for CCN prediction, *Atmos. Chem. Phys.*, 16, 15709-15740,
947 doi:<https://doi.org/10.5194/acp-16-15709-2016>, 2016.

948 Qin, Y., Wang, H., Wang, Y., Lu, X., Tang, H., Zhang, J., Li, L., and Fan, S.: Wildfires in Southeast Asia
949 pollute the atmosphere in the northern South China Sea, *Sci Bull (Beijing)*, 69, 1011-1015,
950 doi:<https://doi.org/10.1016/j.scib.2024.02.026>, 2024.

951 Quinn, P. K., Bates, T. S., Coffman, D. J., and Covert, D. S.: Influence of particle size and chemistry on
952 the cloud nucleating properties of aerosols, *Atmos. Chem. Phys.*, 8, 1029-1042,
953 doi:<https://doi.org/10.5194/acp-8-1029-2008>, 2008.

954 Quinn, P. K., Bates, T. S., Coffman, D. J., Upchurch, L., Johnson, J. E., Moore, R., Ziemba, L., Bell, T.
955 G., Saltzman, E. S., Graff, J., and Behrenfeld, M. J.: Seasonal Variations in Western North Atlantic
956 Remote Marine Aerosol Properties, *J Geophys Res-Atmos*, 124, 14240-14261,
957 doi:<https://doi.org/10.1029/2019jd031740>, 2019.

958 Rose, D., Nowak, A., Achtert, P., Wiedensohler, A., Hu, M., Shao, M., Zhang, Y., Andreae, M. O., and
959 Pöschl, U.: Cloud condensation nuclei in polluted air and biomass burning smoke near the mega-city
960 Guangzhou, China - Part 1: Size-resolved measurements and implications for the modeling of aerosol
961 particle hygroscopicity and CCN activity, *Atmos. Chem. Phys.*, 10, 3365-3383,
962 doi:<https://doi.org/10.5194/acp-10-3365-2010>, 2010.

963 Ross, K. E., Piketh, S. J., Bruinjes, R. T., Burger, R. P., Swap, R. J., and Annegarn, H. J.: Spatial and
964 seasonal variations in CCN distribution and the aerosol-CCN relationship over southern Africa, *J*
965 *Geophys Res-Atmos*, 108, doi:<https://doi.org/10.1029/2002jd002384>, 2003.

966 Sarangi, B., Ramachandran, S., Rajesh, T. A., and Dhaker, V. K.: Black carbon linked aerosol hygroscopic
967 growth: Size and mixing state are crucial, *Atmos Environ.*, 200, 110-118,
968 doi:<https://doi.org/https://doi.org/10.1016/j.atmosenv.2018.12.001>, 2019.

969 Schmale, J., Henning, S., Decesari, S., Henzing, B., Keskinen, H., Sellegri, K., Ovadnevaite, J., Pöhlker,
970 M. L., Brito, J., Bougiatioti, A., Kristensson, A., Kalivitis, N., Stavroulas, I., Carbone, S., Jefferson, A.,

Deleted: Safai, P. D., Raju, M. P., Rao, P. S. P., and Pandithurai, G.: Characterization of carbonaceous aerosols over the urban tropical location and a new approach to evaluate their climatic importance, *Atmos Environ*, 92, 493-500, doi:<https://doi.org/10.1016/j.atmosenv.2014.04.055>, 2014.

977 Park, M., Schlag, P., Iwamoto, Y., Aalto, P., Aijala, M., Bukowiecki, N., Ehn, M., Frank, G., Frohlich, R.,
978 Frumau, A., Herrmann, E., Herrmann, H., Holzinger, R., Kos, G., Kulmala, M., Mihalopoulos, N., Nenes,
979 A., O'Dowd, C., Petaja, T., Picard, D., Pohlker, C., Poschl, U., Poulain, L., Prevot, A. S. H., Swietlicki,
980 E., Andreae, M. O., Artaxo, P., Wiedensohler, A., Ogren, J., Matsuki, A., Yum, S. S., Stratmann, F.,
981 Baltensperger, U., and Gysel, M.: Long-term cloud condensation nuclei number concentration, particle
982 number size distribution and chemical composition measurements at regionally representative
983 observatories, *Atmos. Chem. Phys.*, 18, 2853-2881, doi:<https://doi.org/10.5194/acp-18-2853-2018>, 2018.
984 Seinfeld, J. H. and Pandis, S. N.: *Atmospheric Chemistry and Physics: From Air Pollution to Climate*
985 *Change*, Wiley 2016.
986 Sihto, S. L., Mikkila, J., Vanhanen, J., Ehn, M., Liao, L., Lehtipalo, K., Aalto, P. P., Duplissy, J., Petaja,
987 T., Kerminen, V. M., Boy, M., and Kulmala, M.: Seasonal variation of CCN concentrations and aerosol
988 activation properties in boreal forest, *Atmos. Chem. Phys.*, 11, 13269-13285,
989 doi:<https://doi.org/10.5194/acp-11-13269-2011>, 2011.
990 Sun, Q., Liang, B., Cai, M., Zhang, Y., Ou, H., Ni, X., Sun, X., Han, B., Deng, X., Zhou, S., and Zhao,
991 J.: Cruise observation of the marine atmosphere and ship emissions in South China Sea: Aerosol
992 composition, sources, and the aging process, *Environ. Pollut.*, 316, 120539,
993 doi:<https://doi.org/10.1016/j.envpol.2022.120539>, 2023.
994 Wang, B., Huang, F., Wu, Z., Yang, J., Fu, X., and Kikuchi, K.: Multi-scale climate variability of the
995 South China Sea monsoon: A review, *Dynam Atmos Oceans*, 47, 15-37,
996 doi:<https://doi.org/10.1016/j.dynatmoce.2008.09.004>, 2009.
997 Wang, Y. Q.: *MeteoInfo: GIS software for meteorological data visualization and analysis*, *Meteorol. Appl.*,
998 21, 360-368, doi:<https://doi.org/10.1002/met.1345>, 2014.
999 Xiao, H.-W., Xiao, H.-Y., Luo, L., Shen, C.-Y., Long, A.-M., Chen, L., Long, Z.-H., and Li, D.-N.:
1000 Atmospheric aerosol compositions over the South China Sea: temporal variability and source
1001 apportionment, *Atmos. Chem. Phys.*, 17, 3199-3214, doi:<https://doi.org/10.5194/acp-17-3199-2017>,
1002 2017.

Deleted: Wang, Y., Chen, J., Wang, Q., Qin, Q., Ye, J., Han, Y., Li, L., Zhen, W., Zhi, Q., Zhang, Y., and Cao, J.: Increased secondary aerosol contribution and possible processing on polluted winter days in China, *Environ Int*, 127, 78-84, doi:<https://doi.org/10.1016/j.envint.2019.03.021>, 2019.

008
009

Table 1. The number concentration of particle and cloud condensation nuclei at different supersaturation (SS), the hygroscopicity and **bulk activation ratio (AR)**, and **activation diameter (D_{50})** at different SS in different studies.

Location	period	N_{CN} (cm^{-3})	N_{CCN} (cm^{-3})	Hygroscopicity (κ)	Bulk AR	D_{50} (nm)	Reference
South China Sea	2021.05.05-	6966±9249	2640±3639 (0.20% SS)	0.47±0.21 (0.20% SS)	0.37±0.16 (0.20% SS)	96±19 (0.20% SS)	This study
	2021.06.09		4392±6415 (0.40% SS)	0.54±0.21 (0.40% SS)	0.63±0.17 (0.40% SS)	57±9 (0.40% SS)	
			5215±6862 (0.70% SS)	0.87±0.17 (0.70% SS)			
<u>Northern</u>			1086±691 (0.10% SS)	0.50±0.21 (0.10% SS)	0.23±0.09 (0.10% SS)	145±18 (0.10% SS)	
South China Sea	2021.12.19-	4988±3474	1625±1110 (0.20% SS)	0.31±0.10 (0.20% SS)	0.33±0.12 (0.20% SS)	107±13 (0.20% SS)	This study
	2021.12.29		2218±1503 (0.40% SS)	0.19±0.05 (0.40% SS)	0.44±0.13 (0.40% SS)	79±7 (0.40% SS)	
			2797±1883 (0.70% SS)	0.15±0.05 (0.70% SS)	0.55±0.14 (0.70% SS)	59±6 (0.70% SS)	
Northern South China Sea	2018.08.06-2018.08.27	3463	1544 (0.34% SS)	0.40±0.08 (0.34% SS)	/	/	Cai et al., 2020
Remote South China Sea	2012.09.14-2012.09.26	503±455	450±388 (0.14% SS)	0.54±0.14 (0.14% SS)	0.47±0.16 (0.14% SS)	/	Atwood et al., 2017
			675±516 (0.38% SS)	0.50±0.21 (0.38% SS)	0.72±0.17 (0.38% SS)	/	
			698±555 (0.53% SS)	0.79±0.15 (0.53% SS)	0.85±0.13 (0.71% SS)		
Western North Pacific	2015.03.04-2015.03.26	/	/	0.75±0.21 (0.11% SS)	0.40±0.22 (0.11% SS)	/	Kawana et al., 2020
				0.51±0.16 (0.24% SS)	0.50±0.22 (0.24% SS)		
Guangzhou	2014.11-2014.12	/	3103±1913 (0.10% SS)	0.37±0.11 (0.10% SS)	0.26±0.10 (0.10% SS)	156 ± 19 (0.1% SS)	Cai et al., 2018
			5095±2972 (0.20% SS)	0.29±0.09 (0.20% SS)	0.41±0.14 (0.20% SS)	107 ± 17 (0.2% SS)	
			6524±3783 (0.40% SS)	0.18±0.07 (0.40% SS)	0.53±0.15 (0.40% SS)	78 ± 15 (0.4% SS)	

Deleted: .

Formatted: Subscript

Formatted: Subscript

Formatted Table

Deleted: 2019...640±36392993 [1]

Deleted: 43...7±0.167 [6]

Deleted: 49...7±0.42 [4]

Deleted: 4445...392±64157018 [2]

Deleted: 68...3±0.179 [7]

Deleted: 74...4±0.51 [5]

Deleted: 4786...215±68626402 [3]

Deleted: 9...0.172 [8]

Deleted: 1100...086±6911287 [9]

Deleted: 10

Formatted: Centered

Deleted: 78...1110046 [10]

Deleted: 5

Deleted: Northern

Deleted: 2346...218±1503767 [11]

Deleted: 8...0.134 [13]

Deleted: 2921...797±1883917 [12]

Deleted: 60...5±0.146 [14]

			7913±4234 (0.70% SS)	0.15±0.06 (0.70% SS)	0.64±0.13 (0.70% SS)	<u>58 ± 11 (0.7% SS)</u>	
<u>Yellow Sea</u>	<u>2017.04-2017.05</u>	<u>7622±4038</u>	<u>4821±1763 (0.63% SS)</u>	/	/	/	<u>Park et al., 2018</u>

1060

Formatted: Indent: First line: 0 ch

Formatted: Indent: First line: 0 ch

Deleted: Yellow Sea ... [15]

1062 Table 2. The number concentration of particle, cloud condensation nuclei, and bulk activation ratio in
 1063 different periods.

Cluster	Summer			Winter		
	Indochinese Peninsula	Luzon	Marine	Mainland China	Marine	Mixed
N_{CCN} (cm⁻³)						
0.1% SS	\	\	\	1359±669	439±223	945±400
0.2% SS	1200±787	4066±4748	1135±800	2058±1095	614±318	1460±514
0.4% SS	1650±1187	7804±8608	1812±1052	2792±1478	830±424	1801±640
0.7% SS	2239±1367	10480±9741	2515±1523	3514±1841	1024±463	2101±757
N_{CN} (cm⁻³)						
Total	2699±2147	14674±13844	3033±2366	6875±3263	1728±465	2918±1204
Nucleation	111±206	1543±3341	238±426	893±925	214±281	141±191
Aikten	1156±1261	8653±8815	1668±1526	3089±2017	732±337	806±427
Accumulat ion	1434±1444	3764±4157	1121±929	2923±2440	781±313	1975±831
Bulk AR						
0.1% SS	\	\	\	<u>0.21±0.07</u>	<u>0.26±0.10</u>	<u>0.32±0.04</u>
0.2% SS	<u>0.49±0.13</u>	<u>0.31±0.17</u>	<u>0.40±0.13</u>	<u>0.30±0.09</u>	<u>0.36±0.14</u>	<u>0.51±0.05</u>
0.4% SS	<u>0.73±0.09</u>	<u>0.55±0.18</u>	<u>0.68±0.14</u>	<u>0.40±0.10</u>	<u>0.49±0.16</u>	<u>0.63±0.06</u>
0.7% SS	<u>0.98±0.15</u>	<u>0.76±0.16</u>	<u>0.90±0.13</u>	<u>0.50±0.09</u>	<u>0.61±0.18</u>	<u>0.73±0.06</u>

1064

1065

Deleted: and ...loud condensation nuclei, and bulk activation ratio in different periods.. [16]

Formatted Table

Deleted: 1460...359±1670 [17]

Deleted: 464...39±224 [18]

Deleted: 29...40044 [19]

Deleted: 90...7875 [20]

Deleted: 093...4748864 [21]

Deleted: 1112...135±800682 [22]

Deleted: 105...1095974 [23]

Deleted: 49...31862 [24]

Deleted: 99...51448 [25]

Deleted: 1634...650±118721 [26]

Deleted: 8241...86087478 [27]

Deleted: 85...1052142 [28]

Deleted: 3014...1478934 [29]

Deleted: 1...42439 [30]

Deleted: 900...64096 [31]

Deleted: 1968...13671111 [32]

Deleted: 10776...0480±10540 [33]

Deleted: 477...152341 [34]

Deleted: 668 [35]

Deleted: 52...46393 [36]

Deleted: 296...757829 [36]

Formatted: Font: Bold

1132 Table 3. The slope and coefficient of determination (in parentheses) in CCN closure analysis at
 1133 different supersaturations in different periods.

Cluster	Summer			Winter		
	Luzon	Indochinese Peninsula	Marine	Mainland China	Mixed	Marine
Internal scheme						
0.1% SS	\	\	\	0.91 (0.97)	0.72 (0.95)	0.71 (0.94)
0.2% SS	0.83 (0.89)	0.89 (0.81)	0.76 (0.96)	1.13 (0.96)	1.01 (0.99)	0.94 (0.97)
0.4% SS	0.90 (0.96)	0.90 (0.98)	0.89 (0.97)	1.34 (0.97)	1.14 (0.98)	1.04 (0.98)
0.7% SS	0.91 (0.93)	0.96 (0.92)	0.88 (0.98)	1.38 (0.97)	1.16 (0.99)	1.04 (0.96)
External scheme						
0.1% SS	\	\	\	0.80 (0.97)	0.62 (0.95)	0.59 (0.94)
0.2% SS	0.74 (0.88)	0.77 (0.79)	0.80 (0.96)	1.01 (0.97)	0.90 (0.99)	0.81 (0.97)
0.4% SS	0.78 (0.93)	0.80 (0.97)	0.82 (0.96)	1.23 (0.97)	1.05 (0.98)	0.95 (0.98)
0.7% SS	0.80 (0.92)	0.89 (0.92)	0.80 (0.98)	1.24 (0.98)	1.11 (0.99)	1.00 (0.96)

1134
 1135

Deleted: 81 ...1 (0.94) ... [37]

Deleted: 64 ...2 (0.92) ... [38]

Deleted: 65 ...1 (0.95) ... [39]

Deleted: 82 ...3 (0.82) ... [40]

Deleted: 73 ...9 (0.80) ... [41]

Deleted: 79 ...6 (0.91) ... [42]

Deleted: 05

Deleted: 0.93...01 (0.97) ... [43]

Deleted: 79 ...4 (0.89) ... [44]

Deleted: 79 ...0 (0.92) ... [45]

Deleted: 76 ...0 (0.62) ... [46]

Deleted: 80 ...9 (0.92) ... [47]

Deleted: 23

Deleted: 04

Deleted: 01 ...4 (0.95) ... [48]

Deleted: 80 ...1 (0.88) ... [49]

Deleted: 85...(0.95) ... [50]

Deleted: 0...(0.90) ... [51]

Deleted: 26

Deleted: 06

Deleted: 0.97...04 (0.91) ... [52]

Deleted: 97 ...0 (0.95) ... [53]

Deleted: 96...(0.92) ... [54]

Deleted: 97...(0.945) ... [55]

Deleted: 73 ...4 (0.83) ... [56]

Deleted: 63 ...7 (0.76) ... [57]

Deleted: 75 ...0 (0.960) ... [58]

Deleted: 0.98...01 (0.96) ... [59]

Deleted: 99...(0.97) ... [60]

Deleted: 94...(0.89) ... [61]

Deleted: 69 ...8 (0.9385) ... [62]

Deleted: 69 ...0 (0.65) ... [63]

Deleted: 74...(0.961) ... [64]

Deleted: 0.99 ... (0.97) ... [65]

Deleted: 0.99 ... (0.98) ... [66]

Deleted: 7...(0.95) ... [67]

Deleted: 70...(0.9285) ... [68]

Deleted: 80 ...9 (0.53) ... [69]

Deleted: 72... (0.98) ... [70]

Deleted: 0.99 ... (0.97) ... [71]

Deleted: 0.99

Deleted: 0.96... (0.92) ... [72]

1256 FIGURE CAPTION

1257 Figure 1. The cruises of two shipborne observations, and the location of sample line and chimney of Tan
1258 Kah Kee, and Sun Yat-sen scientific vessel (a); Wind rose of the wind direction and wind speed in
1259 summer and winter cruises; The radius represents the frequency of wind direction occurrences, and the
1260 shaded areas indicate wind speed (b) and (c). The red circles are the midpoints of the ship trajectory
1261 selected for backward trajectory and cluster analysis in summer and the orange squares are the midpoints
1262 of the ship trajectory selected for backward trajectory and cluster analysis in winter.

1263 Figure 2. Timeseries of (a) particle number size distribution, (b) mass concentration of NR-PM₁, and (c)
1264 its fraction, (d) mass concentration of organic carbon and elemental carbon, (e) number concentration of
1265 total particle and cloud condensation nuclei under the supersaturation of 0.1%, 0.2%, 0.4%, and 0.7%,
1266 and (f) aerosol hygroscopicity. The number 1 in figure number means timeseries in summer and number
1267 2 means it in winter.

1268 Figure 3. Particle number size distribution in summer (a) and winter (b); The red markers represent the
1269 activation diameters and hygroscopicity parameters corresponding to 0.1%, 0.2%, 0.4%, and 0.7%
1270 supersaturations in this study (without 0.1% in summer). The green markers represent the hygroscopicity
1271 parameters reported in Atwood et al. (2017) for the southern South China Sea during summer. The gray
1272 markers represent the hygroscopicity parameters documented in Cai et al. (2018) for the Pearl River
1273 Delta region during winter. The fraction of NR-PM₁ in summer (c) and winter (d) in this study, in northern
1274 SCS reported by Liang et al. (2021) (e), and in North Pacific reported by Choi et al. (2017) (f).

1275 Figure 4. The cluster analysis result in summer (a), and winter (b). The solid line in summer means cluster
1276 analysis from May 5 to May 24 and the dash line in summer means cluster analysis from May 25 to June
1277 9; The solid line in winter means cluster analysis from Dec 19 to Dec 21 and Dec 27 to Dec 29, and the
1278 dash line in winter means cluster analysis from Dec 22 to Dec 26.

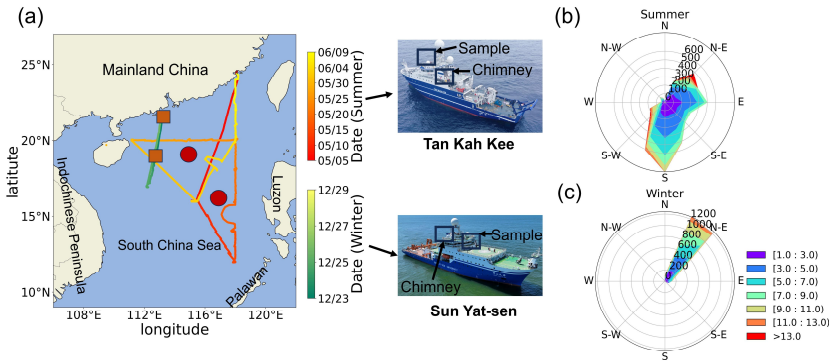
1279 Figure 5. The fraction of NR-PM₁ in "Luzon" period (a), "Indochinese Peninsula" period (b), and
1280 "Marine-s" period (c) in summer. The fraction of NR-PM₁ in "Mainland China" period (d), "Mixed"
1281 period (e), and "Marine-w" period (f) in winter.

1282 Figure 6. The particle number size distribution (PNSD) in "Luzon" period (a), "Indochinese Peninsula"
1283 period (b), and "Marine-s" period (c) in summer. The PNSD in "Mainland China" period (d), "Mixed"
1284 period (e), and "Marine-w" period (f) in winter.

Deleted: ,

1286 Figure 7. The [bulk](#) activation ratio (AR) at different supersaturation (SS) in different periods (a); The
1287 aerosol hygroscopicity (κ) at different supersaturation (SS) in different periods (b).
1288 Figure 8. The normalized mean bias (NMB) calculated by “Internal-mixed” scheme and “External-mixed”
1289 scheme according to CCN closure method. The marker of circle means “Internal-mixed” scheme and the
1290 marker of triangle means “External-mixed” scheme. Different colors means different supersaturations.
1291

1292



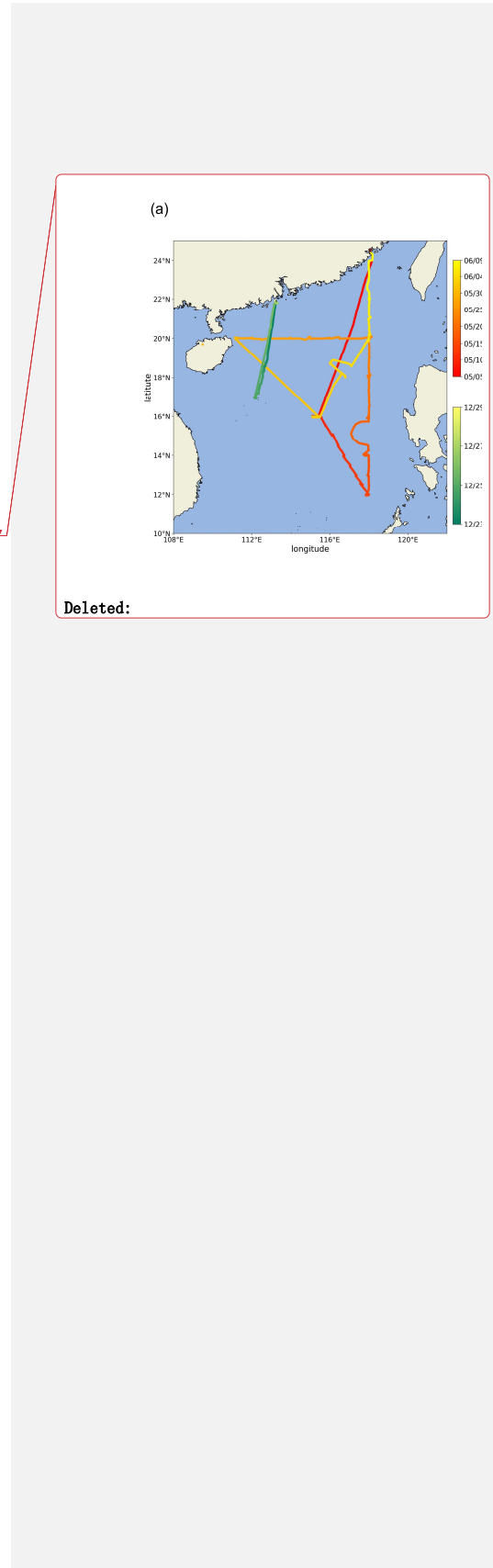
1293

1294

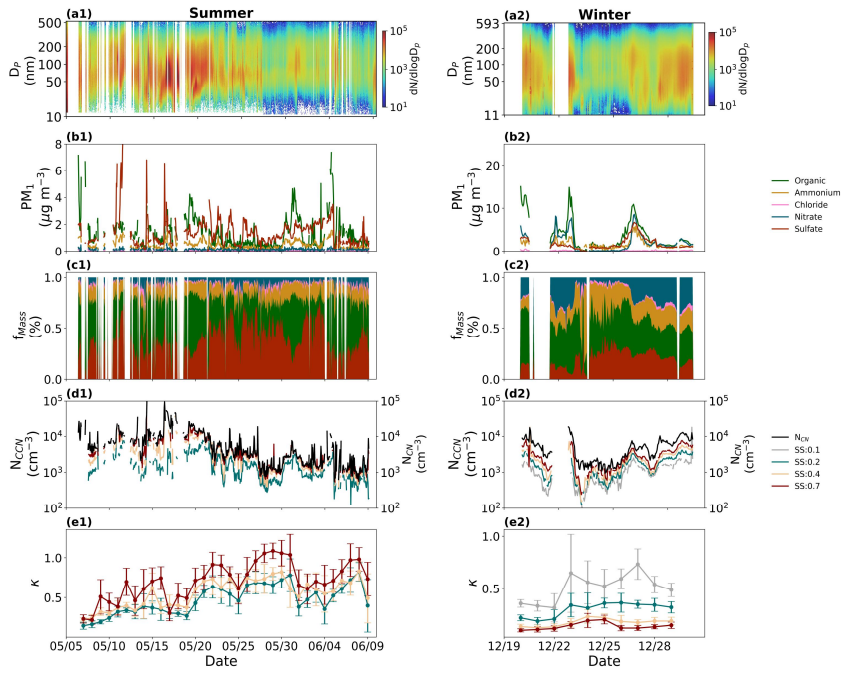
1295

1296

Fig. 1



1298

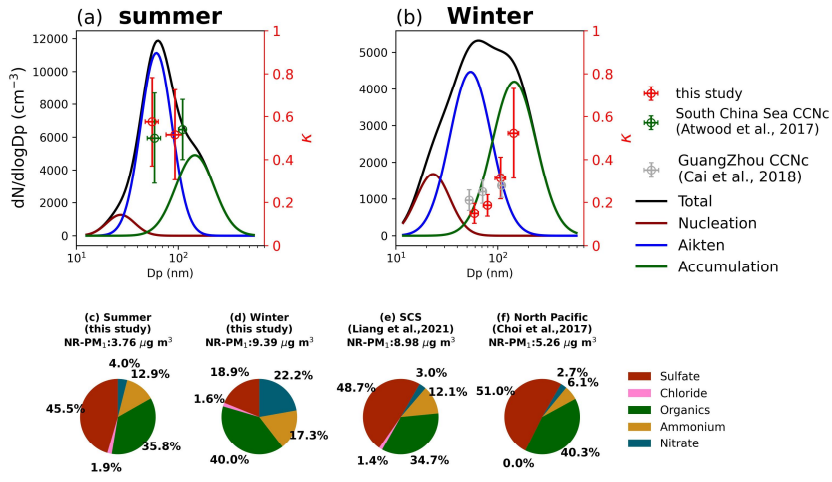


1299

1300 Fig. 2

1301

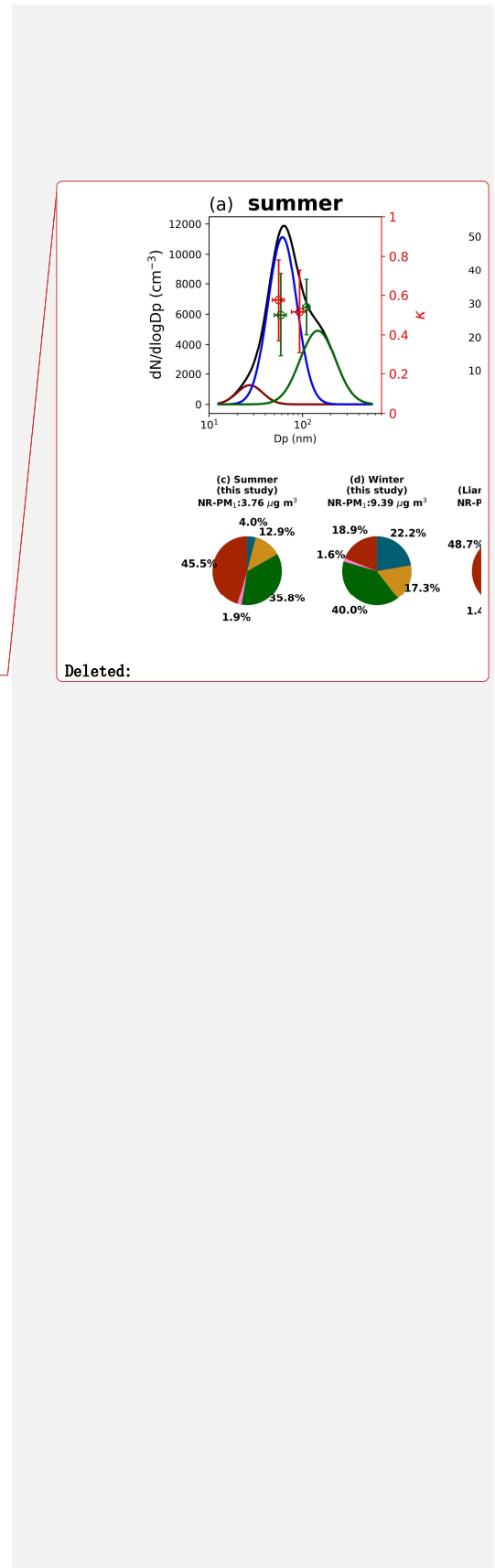
1302

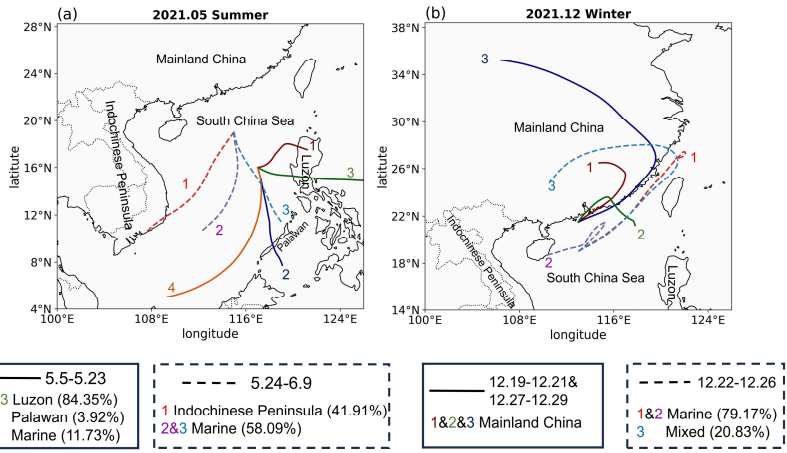


1303

1304 Fig. 3

1305

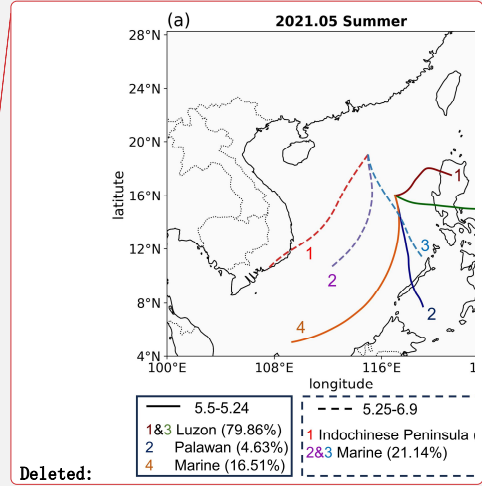




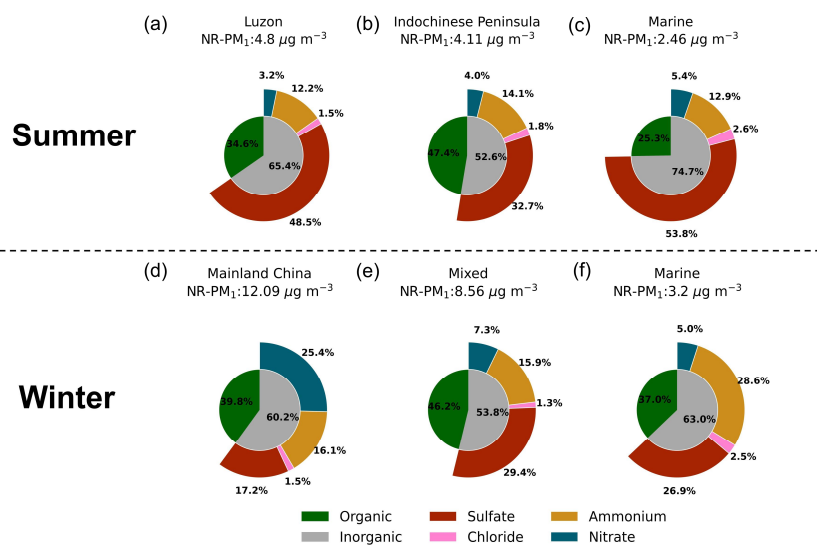
307

1308 Fig. 4

1309



1311

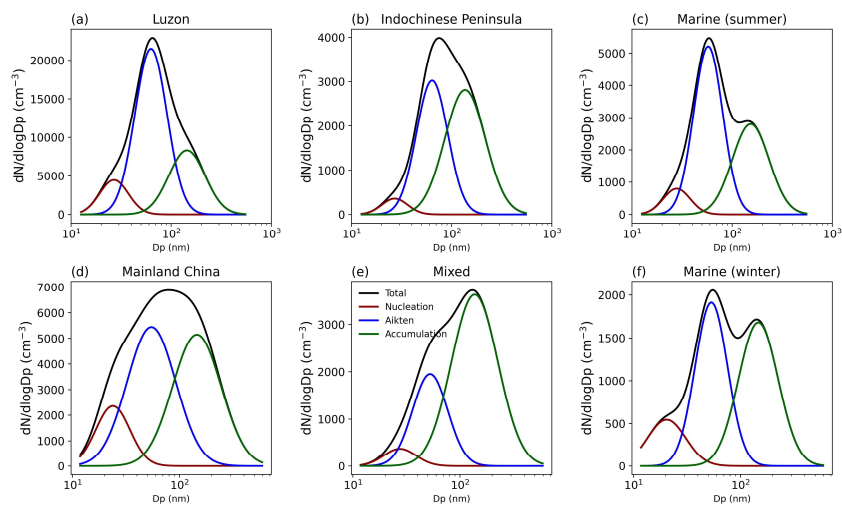


1312

1313 Fig.5

1314

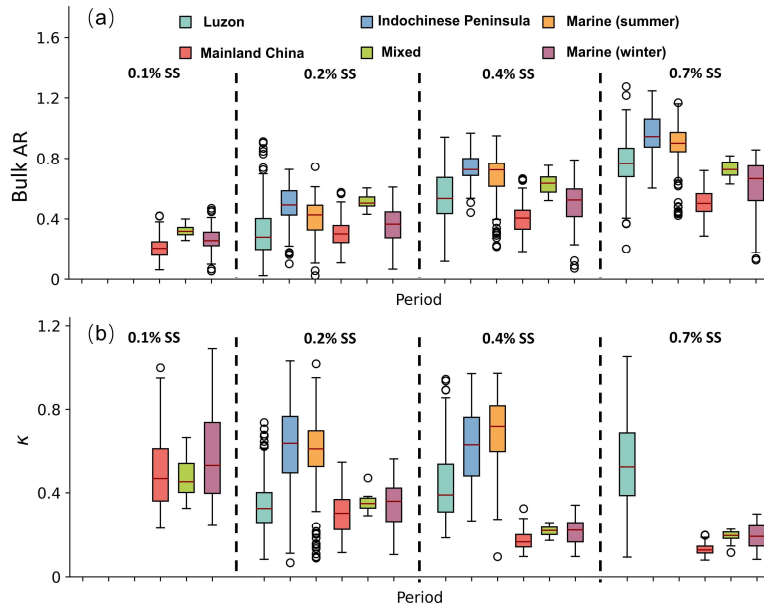
1315



1316
1317
1318

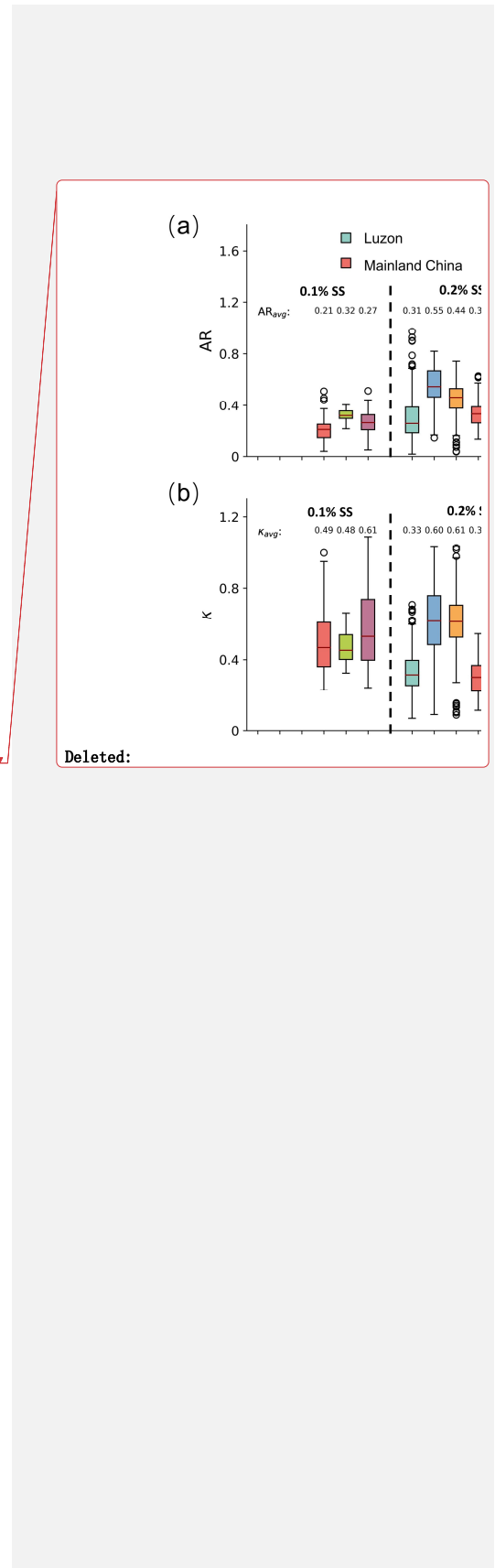
Fig. 6

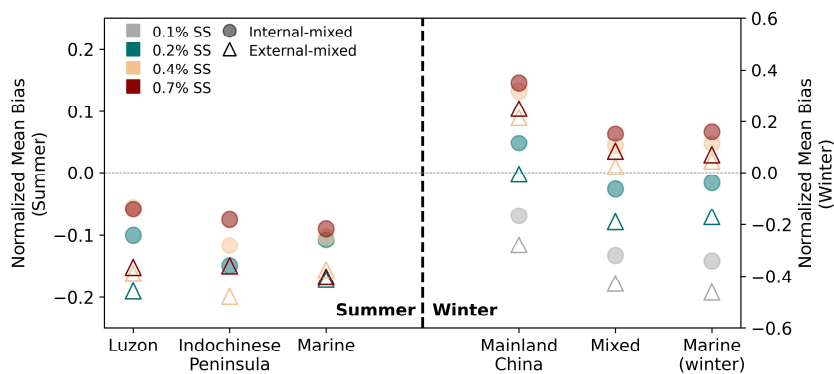
1319



1320
1321
1322

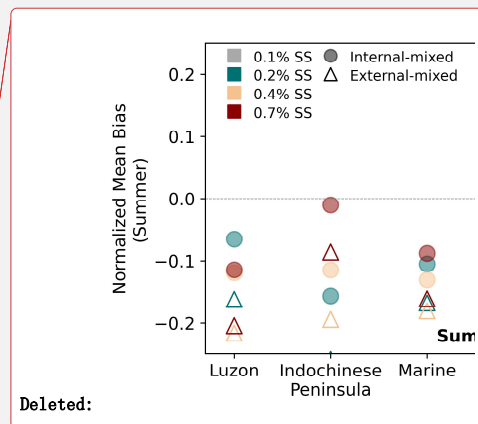
Fig. 7





324
325

Fig. 8.



Deleted:

Moved up [1]: Beddows, D. C. S., Harrison, R. M., Green, D. C., and Fuller, G. W.: Receptor modelling of both particle composition and size distribution from a background site in London, UK, *Atmos. Chem. Phys.*, 15, 10107-10125, doi:<https://doi.org/10.5194/acp-15-10107-2015>, 2015.

Chao, Q., Xiao, C., Li, w., Wang, L., Sun, L., Chen, X., Chen, Y., Li, Y., Gao, G., Liu, Y., Zhang, D., Ai, W., Chen, Y., Cui, T., Dai, T., Feng, A., Guo, Y., Huang, D., Jiang, Y., Li, D., Li, M., Liu, B., Liu, Y., Lv, Z., Mei, m., Wang, Q., Wang, Y., Yin, Y., Zeng, H., Zhang, Y., Zhai, J., Zhao, L., Zhi, R., Zhong, H., Zhou, X., Zhou, X., Zhu, X., and Wu, H.: China Climate Bulletin (2022), China Meteorological Administration, https://www.cma.gov.cn/zfxgk/gkqr/qxbg/202303/t20230324_5396394.html, 2022.

Deleted:

Chao, Q., Xiao, C., Li, w., Wang, L., Sun, L., Chen, X., Chen, Y., Li, Y., Gao, G., Liu, Y., Zhang, D., Ai, W., Chen, Y., Cui, T., Dai, T., Feng, A., Guo, Y., Huang, D., Jiang, Y., Li, D., Li, M., Liu, B., Liu, Y., Lv, Z., Mei, m., Wang, Q., Wang, Y., Yin, Y., Zeng, H., Zhang, Y., Zhai, J., Zhao, L., Zhi, R., Zhong, H., Zhou, X., Zhou, X., Zhu, X., and Wu, H.: China Climate Bulletin (2022), China Meteorological Administration, https://www.cma.gov.cn/zfxgk/gkqr/qxbg/202303/t20230324_5396394.html, 2022.

Huang, S., Wu, Z., Wang, Y., Poulain, L., Höpner, F., Merkel, M., Herrmann, H., and Wiedensohler, A.: Aerosol ... [73]